PALEOCEANOGRAPHY, VOL. 16, NO. 4, PAGES 368–389, AUGUST 2001

Sedimentation rates in the Makarov Basin, central Arctic Ocean: A paleomagnetic and rock magnetic approach

Norbert R. Nowaczyk
GeoForschungsZentrum Potsdam, Projektbereich 3.3, Laboratory for Paleo- and Rock Magnetism, Potsdam, Germany

Thomas W. Frederichs
Fachbereich Geowissenschaften, Universität Bremen, Bremen, Germany

Heidi Kassens, Nils Nørgaard-Pedersen, and Robert F. Spielhagen
GEOMAR, Kiel, Germany

Rüdiger Stein and Dominik Weiel
Alfred-Wegener-Institute for Polar and Marine Research, Columbusstrasse, D-27568 Bremerhaven, Germany

Abstract. Three long sediment cores from the Makarov Basin have been subjected to detailed paleomagnetic and rock magnetic analyses. Investigated sediments are dominated by normal polarity including short reversal excursions, indicating that most of the sediments are of Brunhes age. In general, the recovered sediments show only low to moderate variability in concentration and grain size of the remanence-carrying minerals. Estimations of relative paleointensity variations yielded a well-documented succession of pronounced lows and highs that could be correlated to published reference curves. However, together with five accelerator mass spectrometry ^{14}C ages and an incomplete ^{10}Be record, still two different interpretations of the paleomagnetic data are possible, with long-term sedimentation rates of either 1.3 or 4 cm kyr^{-1}. However, both models implicate highly variable sedimentation rates of up to 10 cm kyr^{-1}, and abrupt changes in rock magnetic parameters might even indicate several hiatuses.

1. Introduction

Chronostratigraphic investigations of Arctic Ocean sediments often suffer from the fact that the sediments are mostly barren of biogenic relicts. Owing to low bioproductivity and additional carbonate dissolution, foraminifers are rarely found, so that neither direct dating through the accelerator mass spectrometry (AMS) ^{14}C method nor oxygen isotope stratigraphy can be performed. On the other hand, the almost purely lithogenic deposits generally carry a strong magnetization. Therefore magnetostratigraphic investigations, i.e., determination of the magnetization directions as well as characterization of the magnetic minerals by detailed rock magnetic analyses, offer a powerful stratigraphic tool. Depending on the sedimentation rate, the succession of major reversals, such as the Matuyama Brunhes reversal, or short-lived geomagnetic reversal excursions within the Brunhes Chron, such as the Laschamp [*Bonhommet and Babkine*, 1967; *Gillot et al.*, 1979] or the Blake [*Smith and Foster*, 1969] excursions, can, in principle, provide a more or less detailed age model. Just these short reversal excursions were frequently found in Arctic marine sediments: Iceland Sea [*Bleil and Gard*, 1989; *Nowaczyk and Frederichs*, 1999; *Völker et al.* [1999], Greenland Sea [*Nowaczyk and Antonow*, 1997; *Nowaczyk*, 1997], Norwegian Sea [*Bleil*, 1989], and Fram Strait, Barents Sea, and eastern Arctic Ocean [*Løvlie et al.*, 1986; *Nowaczyk and Baumann*, 1992; *Nowaczyk et al.*, 1994; *Schneider et al.*, 1996; *Nowaczyk and Knies*, 2000; *Knies et al.*, 2000]. In this paper we present the first high-resolution magnetostratigraphic results on long records from the Makarov Basin, central Arctic Ocean. Besides a correlation of the rock magnetic properties and paleomagnetic directions we also applied the determination of relative paleointensity variations of the geomagnetic field [e.g., *Tauxe and Valet*, 1989; *Tauxe*, 1993]. A stack of 33 relative paleointensity records with different temporal resolution from nearly all over the globe covering the time interval back to 800 ka created by *Guyodo and Valet* [1999] proved that the Earth's magnetic field intensity was highly variable throughout the geologic history. This medium resolution "SINT800" stack, generally characterized by a succession of pronounced lows and highs, provides a new magnetochronostratigraphic reference database that is not based on the directional but intensity variations of the geomagnetic field. Individual, high-resolution relative paleointensity records, such as the Ocean Drilling Program (ODP) 983 record [*Channell et al.*, 1997], can even give a much more detailed image of the geomagnetic field variations than the stacked data and can therefore provide an even more detailed reference frame for dating sedimentary sequences of Brunhes age. However, our intention is not to provide a further paleointensity data set for reference but to derive an age model of the Makarov Basin sedimentary records by using paleointensity variations as a "global correlation tool," as suggested by, for example, *Channell et al.* [2000] or *Stoner et al.* [2000].

Paper number 2000PA000521.
0883-8305/01/2000PA000521$12.00

2. Geological Settings

The triangular-shaped Makarov Basin, with a maximum depth of ~3950 m, is ~500 km wide along the East Siberian Shelf and narrows toward Ellesmere Island. As part of the Amerasian Basin it represents one of the major bathymetric features of the central Arctic Ocean, consisting of the Wrangel and Siberia Abyssal Plains, which are flanked by the Lomonosov, Alpha, and Mendeleev Ridges and bordered by the Siberian and Canadian Shelves [*Weber and Sweeney*, 1990] (Figure 1). The Makarov Basin is bisected by the Marvin spur, a long, steep escarpment. It is covered by perennial sea ice of 2–3 m thickness [*Jokat et al.*, 1999;

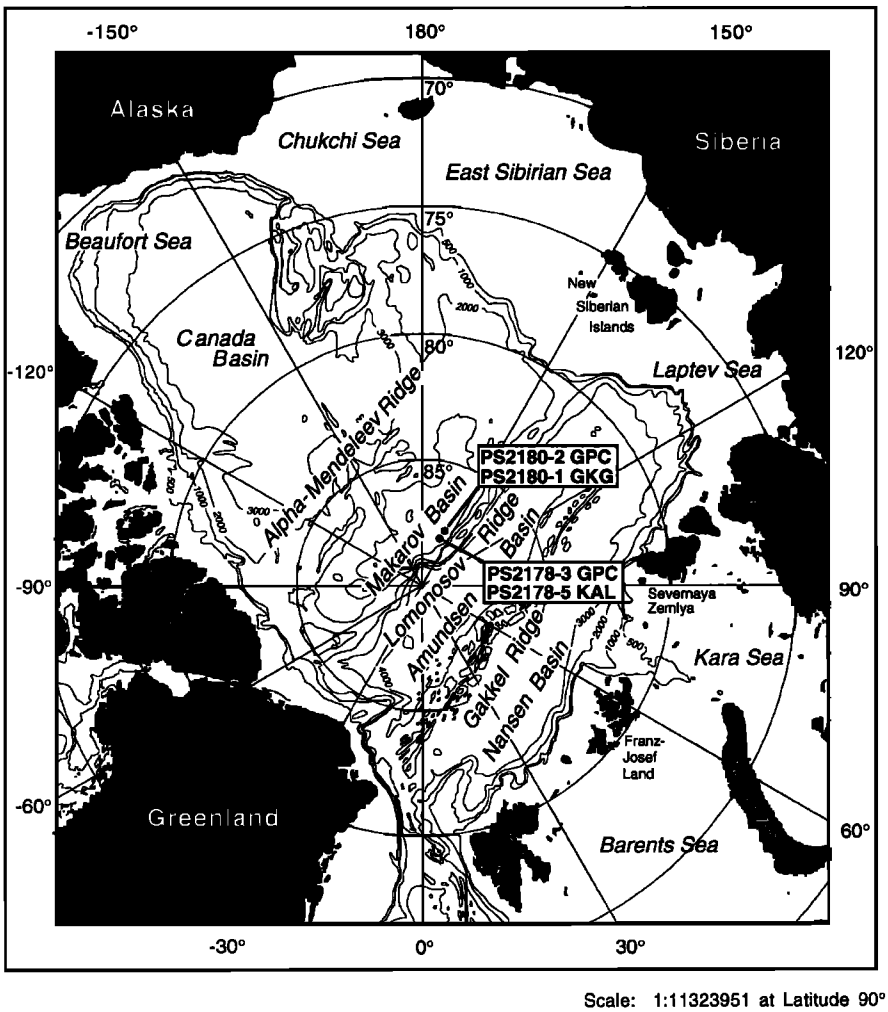

Figure 1. Coring sites in the Arctic Ocean.

Rothrock et al., 1999] driven by the main drift patterns of the Beaufort Gyre and/or the Transpolar Drift [*Reimnitz et al.*, 1992].

The Makarov Basin probably evolved parallel to the opening of the Canada Basin by either seafloor spreading and rotational rifting [*Grantz et al.*, 1990] or crustal extension processes [*Coles and Taylor*, 1990 during Late Cretaceous (Hauterive) and earliest Tertiary, i.e., between ~120 and 56 Ma. It experienced tensional faulting during or shortly after the formation before most of the overlying sediments were deposited [*Weber and Sweeney*, 1990]. The Makarov Basin is incompletely filled with sedimentary deposits of ~3.5–6 km thickness of well-defined horizontally stratified, unconsolidated sediments. They were obviously deposited from turbidity currents that flowed from the East Siberian Shelf across Wrangel Abyssal Plain onto the Siberia Abyssal Plain, where they are interspersed with glacial marine material [*Weber and Sweeney*, 1990; *Sweeney et al.*, 1990]. The long-term terrigenous input depends on sediment supply from the bordering shelves, frequency of turbidites, rafting of sea and glacial ice, erosion and redeposition of silt- and clay-sized material by current activity (winnowing), and pelagic sedimentation [*Clark et al.*, 1980; *Morris et al.*, 1985; *Jackson et al.*, 1990; *Schäper*, 1994; *Stein et al.*, 1994a; *Stein et al.*, 1994b; *Jokat et al.*, 1999]. Average Holocene sedimentation rates (Table 1) indicate quite different values for the individual units of the central Arctic Ocean.

Table 1. Average Holocene Sedimentation Rates in the Arctic Ocean

Area	Sedimentation Rate, cm kyr^{-1}	Reference[a]
Nansen Basin	0.7–0.8	1
Nansen Basin	2.1–16.9	2
Gakkel Ridge	0.6–1.3	1, 3, 4
Gakkel Ridge	0.7–10	2
Amundsen Basin	0.5 to >2.0	1
Amundsen Basin	0.7–3.7	2
Lomonosov Ridge	0.8–1.1	1
Lomonosov Ridge	0.1–3.0	2
Makarov Basin	0.4	1
Makarov Basin	1.4–2.1	2
Alpha–Mendeleev Ridge	0.1	5
Canada Basin	0.1–0.2	6

[a] References: 1, *Stein et al.* [1994b]; 2, *Gard* [1993]; 3, *Köhler* [1992]; 4, *Mienert et al.* [1990]; 5, *Darby et al.* [1989]; 6, *Scott et al.* [1989].

3. Material and Methods

The coring sites (Table 2) are located in the Makarov Basin near the eastern flank of the Lomonsov Ridge, ~45 km apart (Figure 1). The recovered sediments consist of alternating light brownish

Table 2. Location, Water Depth, Length of Sediment Cores and Sample Spacing of Paleomagnetic Samples Presented in This Study

Core	Type[a]	Latitude, °N	Longitude, °E	Water Depth, m	Recovery, cm	Sample Spacing, cm
PS 2178-3	GPC	88°00.3′	159°10.1′	4009	1372	3
PS 2178-5	KAL	88°01.5′	159°42.2′	4008	831	4
PS 2180-1	GKG	87°37.6′	156°40.5′	4005	48	
PS 2180-2	GPC	87°38.6′	156°58.3′	3991	1296	5

[a] GPC, giant piston corer (diameter Ø of 10 cm, 25 m length); KAL, square barrel Kastenlot corer (30 × 30 cm, 12 m length); GKG, large box corer Grosskastengreifer (50 × 50 cm, 0.6 m height).

sandy silts and light greenish-gray silty clay. The content of total organic carbon (TOC) ranges from 0.1 to 0.5%. The carbonate content is generally very low (<0.2%), with some distinct peaks reaching 6% [*Schubert and Stein*, 1996]. However, below ~15 cm biogenic carbonate, coccoliths or foraminifers are rarely found in the sediments recovered from the Makarov Basin [*Gard*, 1993]. Therefore no stable oxygen isotope curve could be derived from the long cores. Only five AMS ^{14}C ages are available for the box corer PS2180-1 for the upper 15 cm (Table 3).

The cores were sampled with 6.2 cm^3 plastic cubes, each 3–5 cm (Table 2), generally avoiding sandy layers, yielding a total collection of nearly 900 samples. Magnetic volume (low field) susceptibility κ_{LF} of the paleomagnetic samples was measured with a Kappabridge KLY 3S (sensitivity of 1.2×10^{-8} SI). A subcore from the box corer taken at site PS2180 was logged with a Bartington MS2F sensor applying the technique described by *Nowaczyk and Antonow* [1997]. Measurements of the natural remanent magnetization (NRM) were performed with three-axis cryogenic magnetometers. All samples were demagnetized in 8–10 steps with a maximum alternating field (AF) amplitude of 100 mT in order to remove viscous overprints. The characteristic remanent magnetization (ChRM) of each sample was determined by subjecting its demagnetization results to principle component analysis [*Kirschvink*, 1980].

All samples were subjected to some basic rock magnetic analyses. Anhysteretic remanent magnetizations (ARM), as a measure of concentration of magnetic minerals, were generated along the samples' positive z axis with 0.05 mT static field and 100 mT AF amplitude. ARM were also measured with a cryogenic magnetometer and demagnetized at the same AF levels that were used for NRM demagnetization (up to 65 mT). The median destructive field of the ARM (MDF_{ARM}) and the ratio κ_{ARM}/κ_{LF} (κ_{ARM} is anhysteretic susceptibility, ARM intensity, divided by static field amplitude of 0.05 mT) were determined in order to monitor relative magnetic grain size changes of the magnetic fraction. Additional rock magnetic methods were applied to samples from core PS 2180-2. Isothermal remanent magnetizations (IRM) were imprinted with a pulse magnetizer and measured with a fluxgate spinner magnetometer. Then 176 out of 251 samples were stepwise exposed to increasing peak fields of up to 1500 mT along their positive z axis in order to record complete IRM acquisition curves. The remainder of the sample collection was exposed to a field of 1500 mT only. The IRM acquired at 1500 mT is defined as "saturation" isothermal remanence (SIRM). Finally, the intensity ratio of ARM to SIRM was calculated as another estimate of relative magnetic grain size changes. All samples from core PS2180-2 were also used for determination of the anisotropy of magnetic susceptibility using the anisotropy option of the KLY3S; that is, susceptibility is numerously measured while the sample is rotating around the x, y, and z axes, respectively. Measurements from the three orthogonal planes are combined with one bulk measurement in order to create a complete anisotropy tensor, represented by the general susceptibilities K_{max} (maximum), K_{int} (intermediate), and K_{min} (minimum) and their respective orientation angles, declination, and inclination, with respect to sample coordinates. According to *Nowaczyk* [1997], estimations of relative paleointensity variations were calculated by dividing NRM intensities after 50 mT AF demagnetization by (1) the low field magnetic susceptibility κ_{LF}, (2) the SIRM intensity, and (3) ARM intensities, also after demagnetization with 50 mT, and then normalizing each curve to its average.

Table 3. Accelerator Mass Spectrometry (AMS) ^{14}C Ages Determined for Core PS2180-1

Depth, cm	Age, ka	
	Uncalibrated	Calibrated[a]
0.0	2.42	1.99[b]
4.5	7.26	7.67[b]
8.5	16.23	18.74[b]
12.5	35.02	38.60[c]
14.5	37.35	40.85[c]

[a] Radiocarbon ages, after applying a constant reservoir effect of 440 years [*Mangerud and Gulligsen*, 1975], were converted to calendar ages by the CALIB 4.3 calibration program by using the calibration data sets of *Stuiver et al.* [1998] and *Stuiver and Reimer* [1993] and, beyond 20.3 ^{14}C ka, by applying the age shift determined by *Völker et al.* [1998].

[b] Calibration data sets of *Stuiver et al.* [1998] and *Stuiver and Reimer* [1993] were used.

[c] Age shift determined by *Völker et al.* [1998] was used.

4. Results

4.1. Paleomagnetism

The cores were recovered close to the geographic North Pole. Here ChRM declinations apparently show a large scatter because owing to the geomagnetic secular variation the geomagnetic pole can migrate to positions south of the coring sites even during stable phases of the geodynamo [e.g., *Merril and McElhinny*, 1983, Figure 4.4]. Consequently, the paleomagnetic results of the three cores are discussed mainly on basis of the ChRM inclinations (Figure 2), the most significant paleomagnetic parameter at such high latitudes (88°N). ChRM directions in the recovered sediments are clearly dominated by normal polarity, i.e., steep positive inclinations, indicating a Brunhes age for most of the sediments. However, six short intervals of steep negative inclinations are documented within the cores. Below the inclination spike 6 (Figure 2) the directions in the lower ~2 m of the piston cores exhibit only a limited similarity, possibly caused by the coring process. There are also differences in the inclination patterns between the Kastenlot (KAL) and the piston core (GPC) from Site PS2178. Some intervals of the Kastenlot, below inclination events 1 and 3, show scattered shallow inclinations that are less pronounced within the piston core (Figure 2). Another general difference, although both cores originate from the same site (in the limits of keeping the ship's position within drifting sea ice), is that the inclination pattern of the piston core is elongated with respect to the inclination

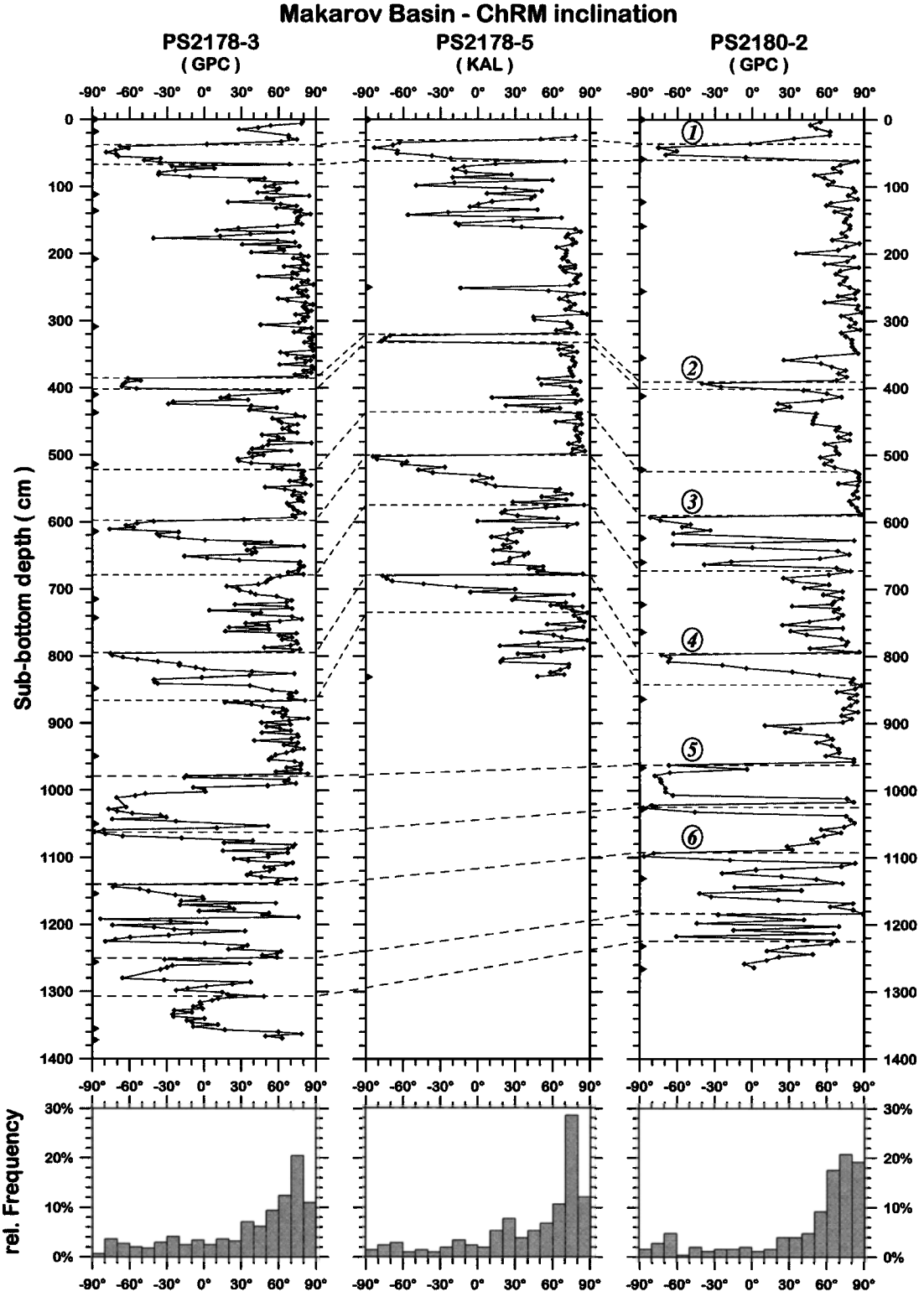

Figure 2. Inclination of the characteristic remanent magnetization (ChRM) of the three long cores from the Makarov Basin. A subset of correlation levels is indicated by dashed lines. Triangles at the left depth axis of each core indicate core breaks. Circled numbers mark intervals of reversed magnetizations as discussed in the text. Histograms at the bottom show the frequency distribution of the ChRM inclinations.

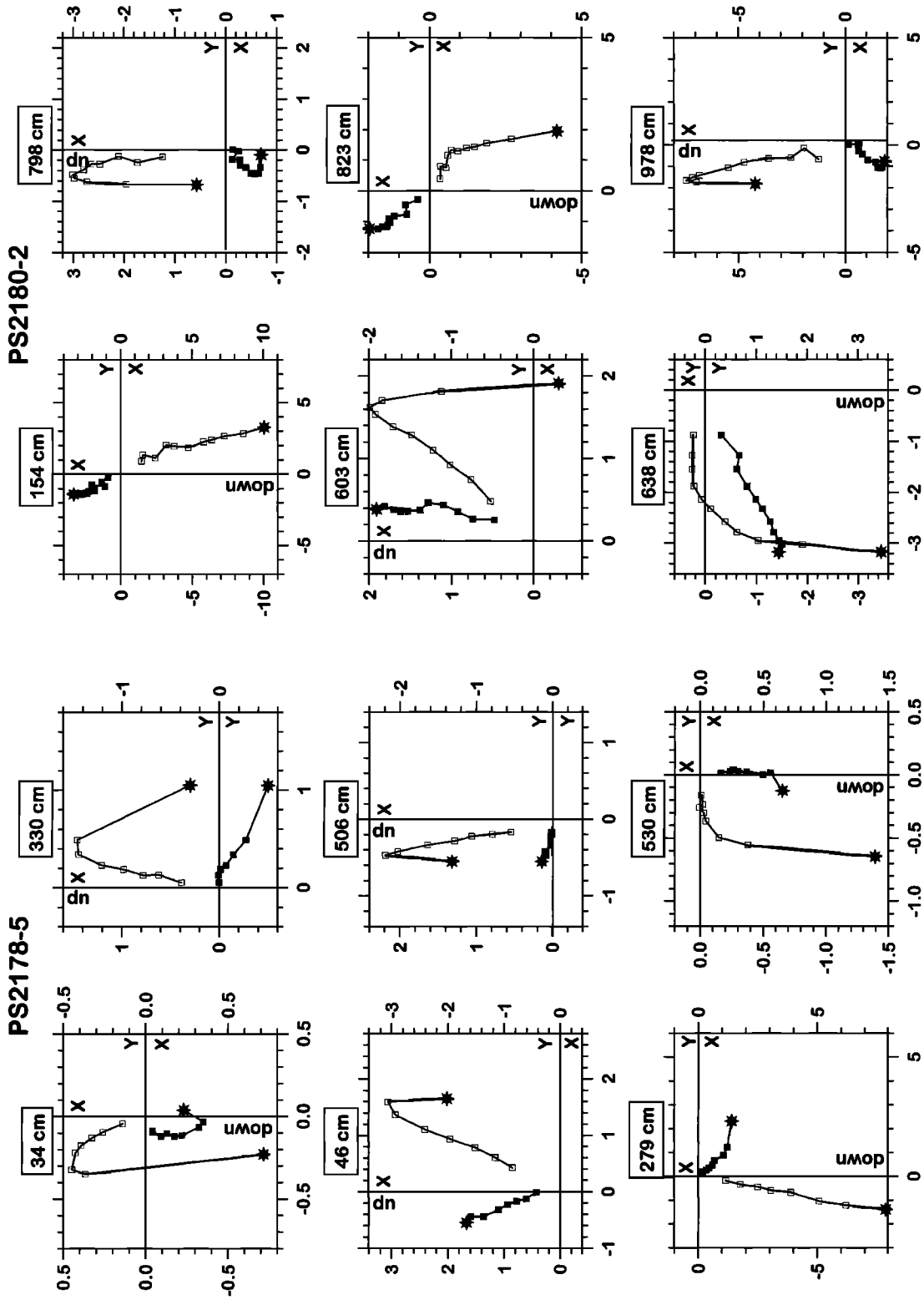

Figure 3. Orthogonal projections of (left) six samples from core PS2178-5 and (right) six samples from core PS2180-2. Solid squares denote the horizontal (*X*-*Y*) plane, and open squares denote a vertical (*X*-*Z* or *Y*-*Z*) plane. The *z* axis is positively pointing downward. The asterisk in each curve denotes the NRM measurement, and axes are absolutely scaled in mA m^{-1}.

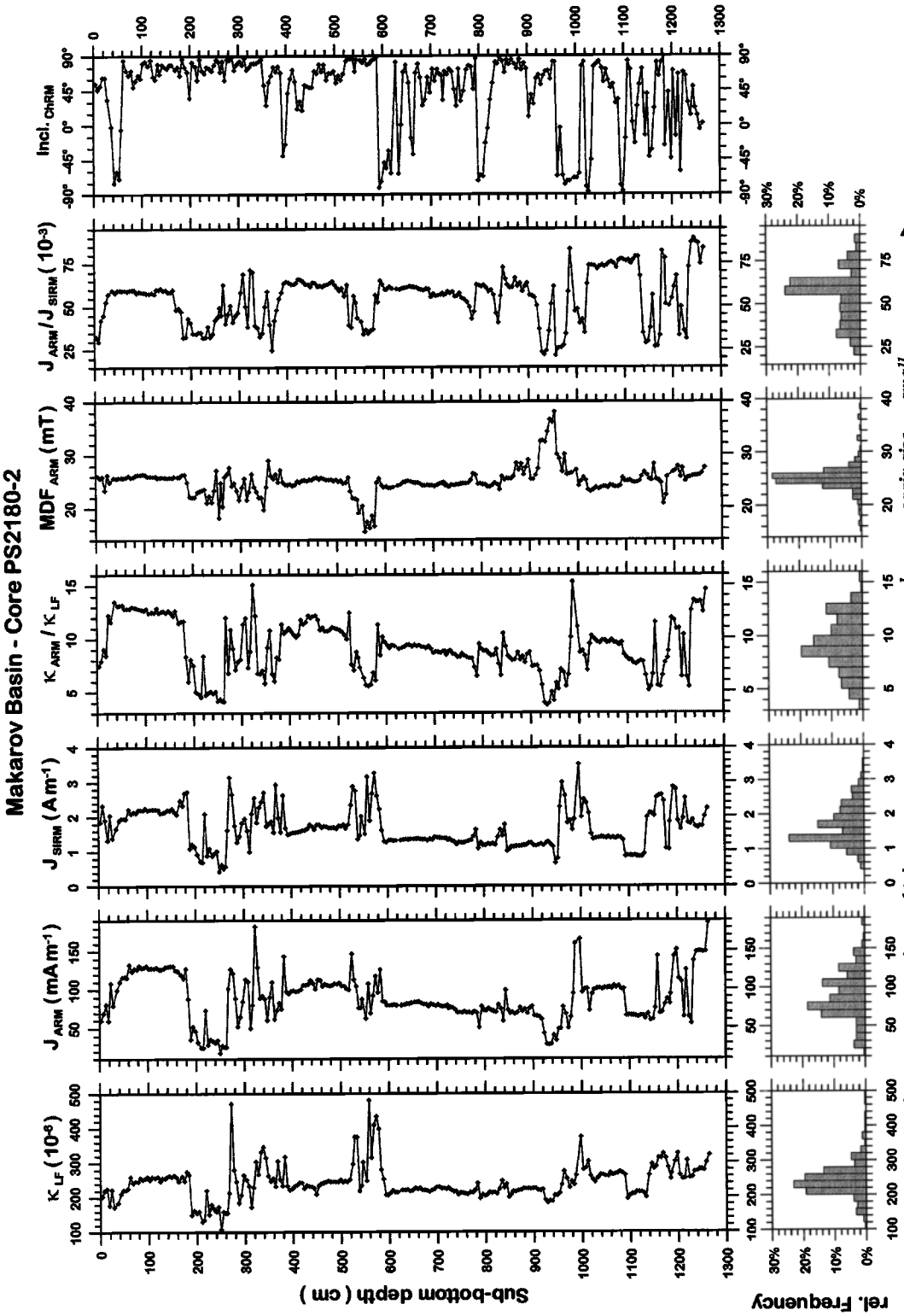

Figure 4. Rock magnetic results from core PS2180-2. Magnetic susceptibility κ_{LF} and intensities of the anhysteretic (J_{ARM}) and saturated isothermal remanent magnetizations (J_{SIRM}) reflect concentration variations. Anhysteretic susceptibility κ_{ARM} (for a definition, see text) over κ_{LF}, median destructive field of ARM (MDF_{ARM}), and ratio of J_{ARM}/J_{SIRM} indicate relative magnetic grain size changes. Histograms summarize the overall variability of the parameters. ChRM inclinations are shown on the right.

pattern of the Kastenlot by ~15%. This is caused by the suction of the piston. An alternative interpretation could be that sediments within the Kastenlot are compressed since it works like a gravity corer. However, recovery of the PS2178 Kastenlot was ~96%, calculated from penetration and length of the recovered core. This allows an estimation of a maximum compaction of 4%, so that the difference between the two cores is more likely due to suction effects in the piston corer.

Correlation of the reversed intervals, supported by information on sediment color and other physical/magnetic properties (see

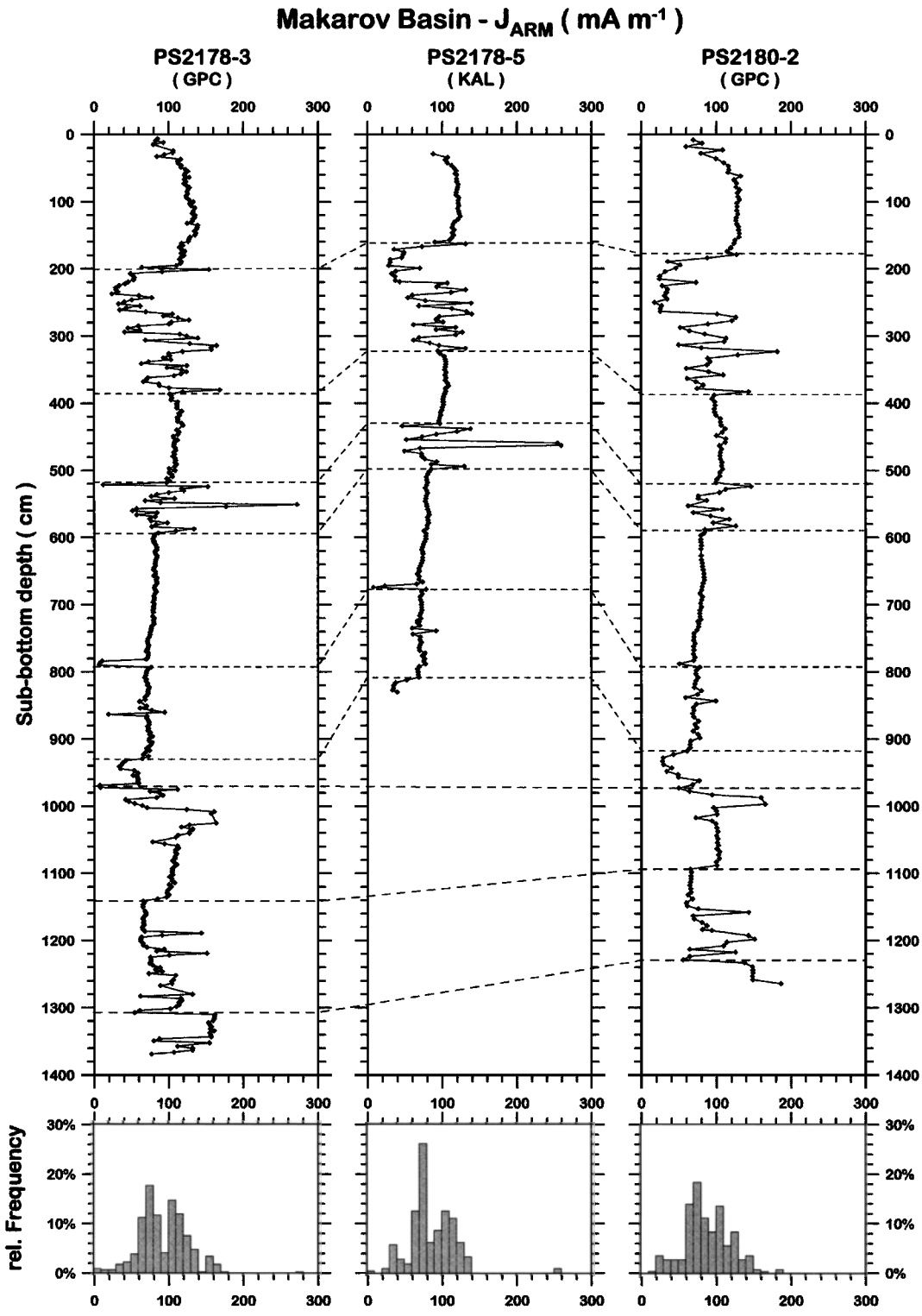

Figure 5. (a) Correlation of down core variation and relative frequencies of ARM intensities J_{ARM} for all three cores from Makarov Basin. (b) Correlation of down core variation and relative frequencies of MDF_{ARM} for Makarov Basin cores.

below), is indicated by the dashed lines in Figure 2. All histograms included in Figure 2 show a maximum at steep positive inclinations. Nondipolar directions, i.e., shallow positive and negative inclinations, are mainly due to samples in transitional intervals between clearly normal (steep positive) and reversed (steep negative) inclinations. However, totally reversed inclinations (70°–90°) are also clearly present.

Orthogonal diagrams of the demagnetization results of six samples from core PS2178-5 and six from core PS2180-2 are shown in Figure 3, respectively. The plots are displayed in mA m^{-1} in order to show that the sample's intensity, even after maximum demagnetization with 100 mT AF amplitude, is still high above the magnetometer's noise level (0.005 mA m^{-1}). The representative results were taken mainly from intervals with

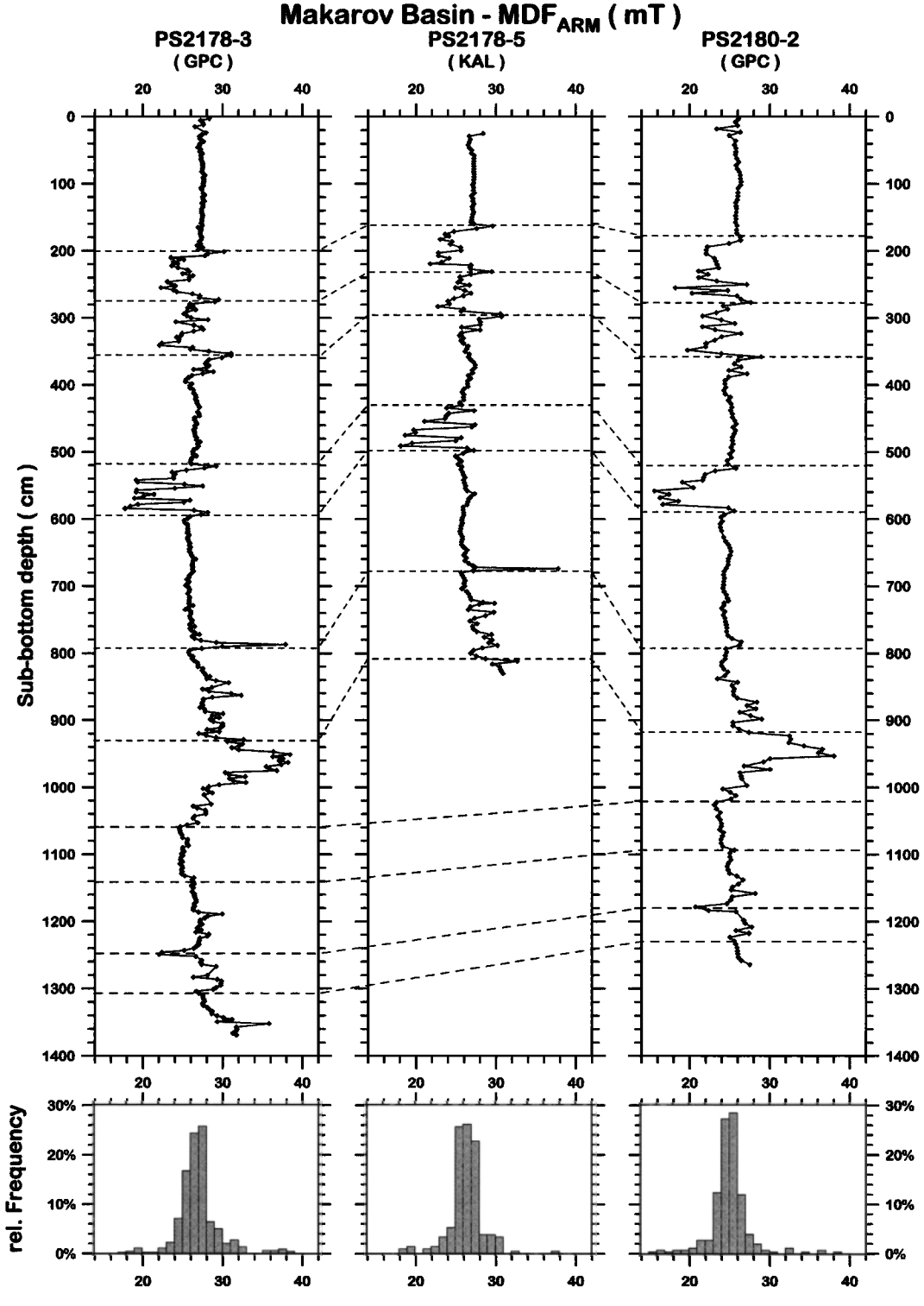

Figure 5. (continued).

negative ChRM inclination, indicating a reversed polarity. Included also are a few examples of samples exhibiting a shallow ChRM inclination, indicative of intermediate field configurations, and two normal polarity samples. In general, despite their type of ChRM inclination, shallow or steep negative, all samples displayed in Figure 3 are characterized by a steep downward directed overprint. This viscous component is parallel to the recent magnetic field direction, with an expected dipole inclination of 88.8°. It could be removed within the first two to five demagnetization steps, equal to AF amplitudes of 20–50 mT. Consequently, mainly the last four demagnetization steps (50–100 mT) were used for determination of the ChRM direction.

4.2. Rock Magnetism

The concentration of magnetic carrier minerals in core PS2180-2 as estimated by magnetic susceptibility κ_{LF}, ARM, and SIRM intensity measurements (Figure 4) partly is extremely constant. For ~60% of the sediments investigated, the associated parameters vary just by a factor of 2–3, whereas the maximum variations do not exceed an order of magnitude. The homogenous sections are also characterized by minimum grain size variations of the magnetic minerals (Figure 4). Especially, the coercivity parameter MDF_{ARM} is very narrow banded. This largely homogeneous magnetomineralogy is linked to pure silty clays. The remaining intervals, with sand contents of up to 30% and occasional mud clasts, show only moderate variability in concentration and grain size, respectively, when compared to the silty clay layers.

The dominant remanence carrier throughout the whole investigated sediment column is (titano-) magnetite, as derived from the obtained IRM acquisition curves, which all reached saturation between 300 and 500 mT. Results from all cores (J_{ARM} and MDF_{ARM}) together with some correlation lines are shown in Figures 5a and 5b, illustrating that all three cores comprise similar variations in rock magnetic properties, down core as well as in amplitude. Nearly all intervals of steep negative ChRM inclinations in core PS2180-2 are parts of sections characterized by extremely homogenous rock magnetic parameters (Figure 4). On the other hand, intervals of larger variability of rock magnetic parameters, generally with a higher sand content, do not show anomalous directions. A final proof that reversed directions most likely document geomagnetic reversal excursions is provided from

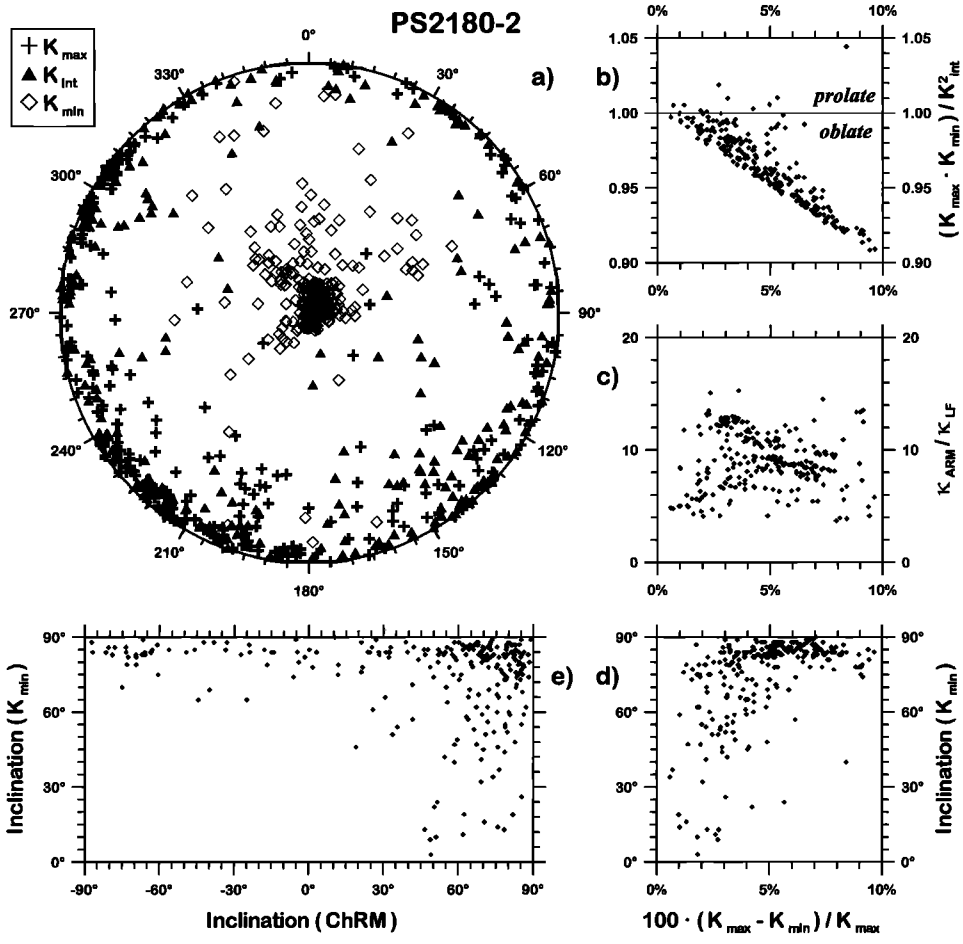

Figure 6. Results from determinations of the anisotropy of magnetic susceptibility performed on all samples (n = 251) from core PS2180-2. (a) Orientations of the principle axes K_{max}, K_{int} and K_{min}, (b) shape ($K_{max}K_{min}/K_{int}^2$) of the anisotropy ellipsoids, (c) relative magnetic grain sizes, represented by κ_{ARM}/κ_{LF}, and (d) inclinations of principle axis K_{min} as a function of degree of anisotropy (100 ($K_{max} - K_{min}$)/K) and (e) ChRM inclinations versus K_{min} inclinations. The data indicate, in most cases, a flat-lying (oblate) ellipsoid, independent from rock magnetic variations. Samples with a low degree of anisotropy or nearly isotropic samples show a random orientation of principle axes. All transitional (shallow) and reversed (steep negative) ChRM inclinations are associated with steep K_{min} inclinations (Figure 6e); that is, they are not associated with an anomalous sedimentary fabric.

data of anisotropy of magnetic susceptibility determined on samples from core PS2180-2. Figure 6a displays the orientation of the three ellipsoid axes K_{max}, K_{int}, and K_{min}. Generally, the K_{max} and K_{int} axes, which are more or less of the same length throughout the whole core, are lying in the horizontal plane, and the K_{min} axes have steep inclinations. The ratio 100 $(K_{max} - K_{min})/K_{max}$, i.e., the maximum degree of anisotropy, reaches values of up to 10% and increases with increasing subbottom depth, whereas the shape of

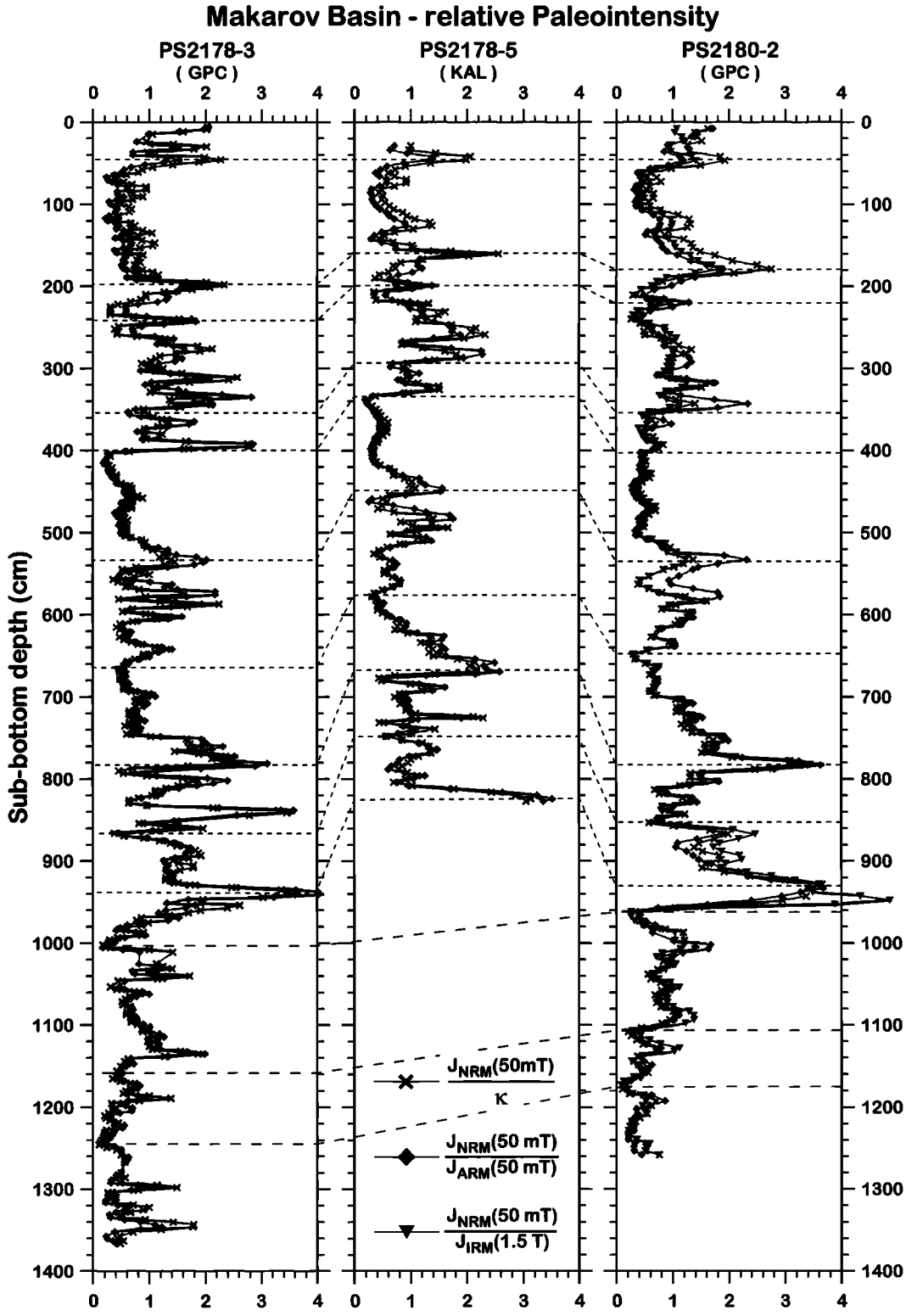

Figure 7. Normalized estimates of relative paleointensity variation, as indicated by the ratios defined in the middle plot. The curves were smoothed with a weighted (triangular) three-point running average. A subset of correlation levels is indicated by dashed lines.

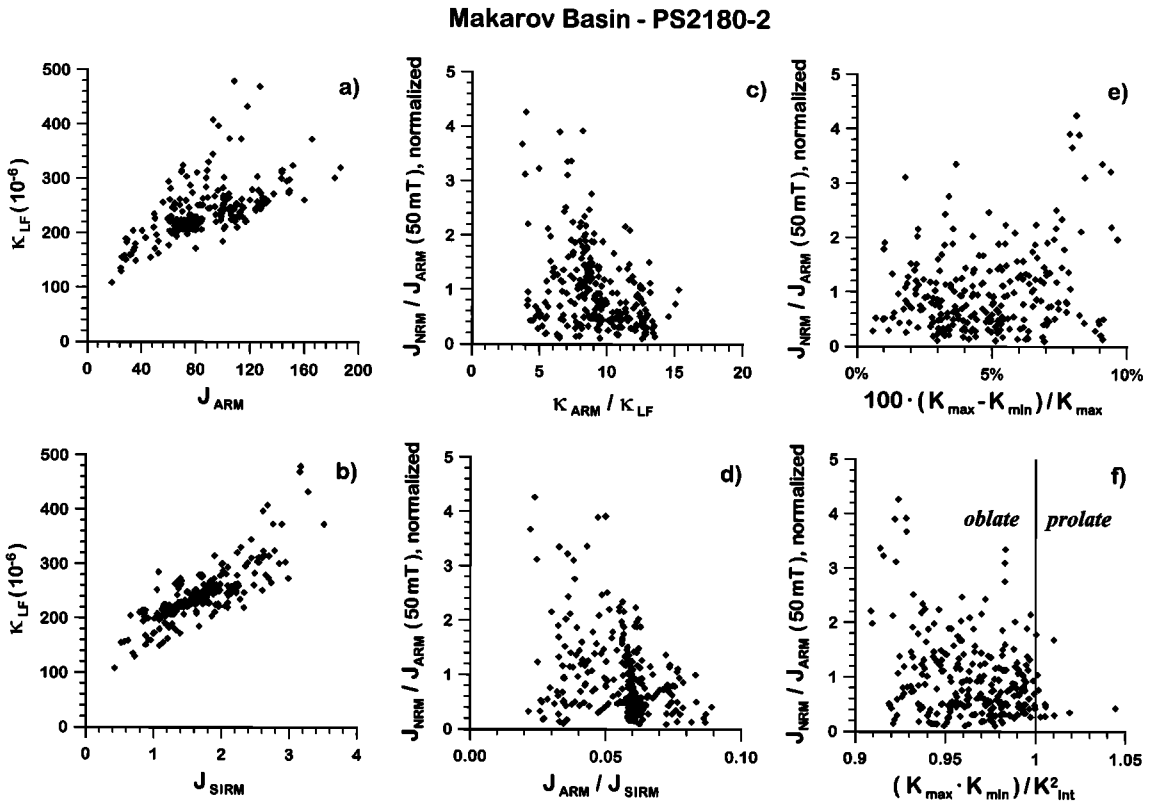

Figure 8. Reliability test of paleointensity estimate for core PS2180-2. Magnetic susceptibility (κ_{LF}) versus (a) ARM intensity J_{ARM} and (b) SIRM intensity J_{SIRM}, relative paleointensity (J_{NRM}/J_{ARM} (50 mT)) versus magnetic grain size indicative parameters (c) κ_{ARM}/κ_{LF} and (d) J_{ARM}/J_{SIRM}, and relative paleointensity versus anisotropy parameters (e) 100 ($K_{max} - K_{min}$)/K_{max} (degree of anisotropy) and (f) ($K_{max}K_{min}$)/K^2_{int}(shape of anisotropy ellipsoid).

the ellipsoid, as estimated by the ratio ($K_{max}K_{min}$)/K^2_{int}, is generally oblate, especially for samples with a stronger anisotropy (Figure 6b). There is no relationship between magnetic grain size variations and the degree of anisotropy, as shown by the diagram κ_{ARM}/κ_{LF} versus 100 ($K_{max} - K_{min}$)/K_{max} (Figure 6c). The inclination of K_{min} is steep for samples with stronger anisotropy, which is very likely due to simple compaction effects, whereas low anisotropy to nearly isotropic samples show random K_{min} inclinations (Figure 6d). However, this simply reflects the fact that the orientations of the three principle axes are less determined for samples that approximate an isotropic status. Therefore, in summary, we take a steep inclination of K_{min} as a clear indicator of an undisturbed sediment fabric. Since all intervals with intermediate (shallow) and steep negative ChRM inclinations are all linked to steep inclinations of the K_{min} axis (Figure 6e), i.e., they are not associated with a disturbed sediment fabric, nonnormal ChRM inclinations can be interpreted as records of geomagnetic field behavior, i.e., short-term reversal excursions, comprising dipolar (steep positive and negative inclinations) and transitional/nondipolar directions (shallow inclinations).

4.3. Paleointensity Estimation

As discussed in section 4.2, the concentration of magnetic carrier minerals in core PS2180-2 vary by less than a factor of 10 (e.g., SIRM ranges from 0.42 to 3.50 A m^{-1}), with most of the concentration related parameters just varying by a factor of 2–3. This qualifies the investigated sediments as an appropriate material for an estimation of relative paleointensity variations of the Earth's magnetic field [*Tauxe*, 1993]. Since secondary overprints

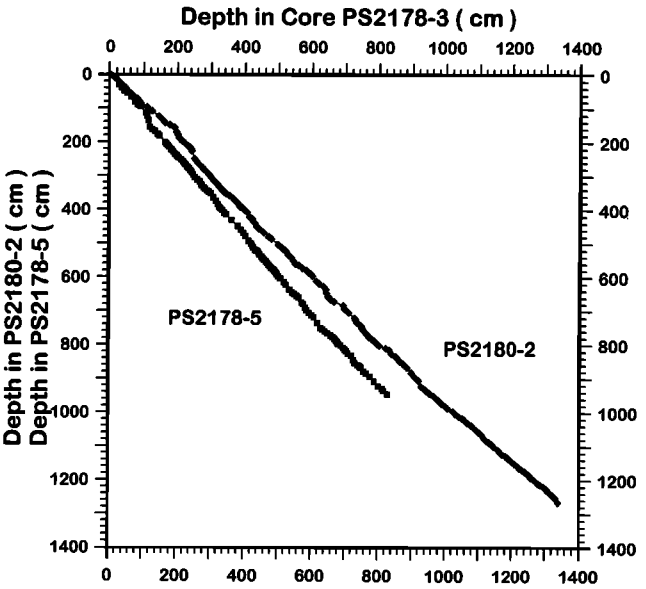

Figure 9. Tie points of the correlation of cores PS2178-5 and PS2180-2 to core PS2178-3, defined as master core. Correlation is based on low field magnetic susceptibility κ_{LF}, ChRM inclination (Figure 2), ARM intensity (Figure 5a), MDF_{ARM} (Figure 5b), estimates of relative paleointensity (J_{NRM} (50 mT)/J_{ARM} (50 mT), Figure 8), and sediment colors.

of the ChRM directions had to be eliminated with AF amplitudes of up to 50 mT (Figure 3), we used NRM intensities at this AF level for paleointensity calculations [see also *Nowaczyk*, 1997]. For the concentration normalization parameter we chose the ARM intensity (also after demagnetization with 50 mT) because the ARM mainly affects fine-grained magnetite particles that are also the main carrier of the paleomagnetic information, whereas low field susceptibility κ_{LF} and saturated isothermal remanent

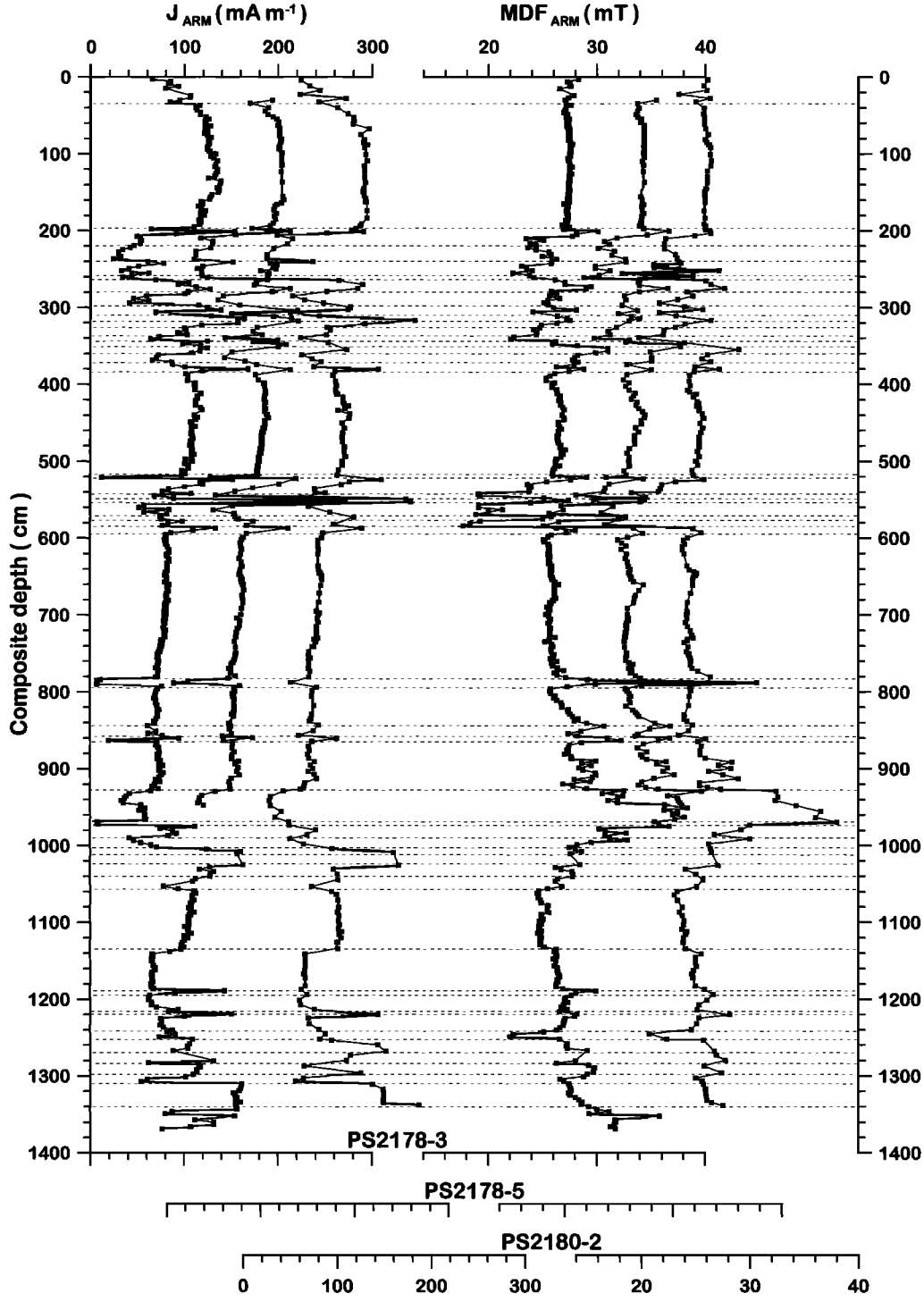

Figure 10. (left) ARM intensity (J_{ARM}) and (right) median destructive field (MDF_{ARM}) after transformation of the depth axes of core PS2178-5 (middle curves in both plots) and PS2180-2 (right curves in both plots) to the depth axis of core PS2178-3 (left curves in both plots), defined as composite depth. Horizontal lines indicate visible changes in lithology.

magnetization (SIRM) are also influenced by multidomain particles that do not contribute to a stable NRM. Moreover, κ_{LF} is also influenced by contributions of the nonmagnetic sediment matrix. However, we also calculated NRM normalizations with κ_{LF} for all three cores, and we calculated SIRM normalizations but only for core PS2180-2 (Figure 7). The morphology of the derived two or three curves are almost the same for each core, independent of the method of normalization, with only little amplitudenal offsets within some depth intervals but with the same succession of peaks and troughs. For the majority of depth

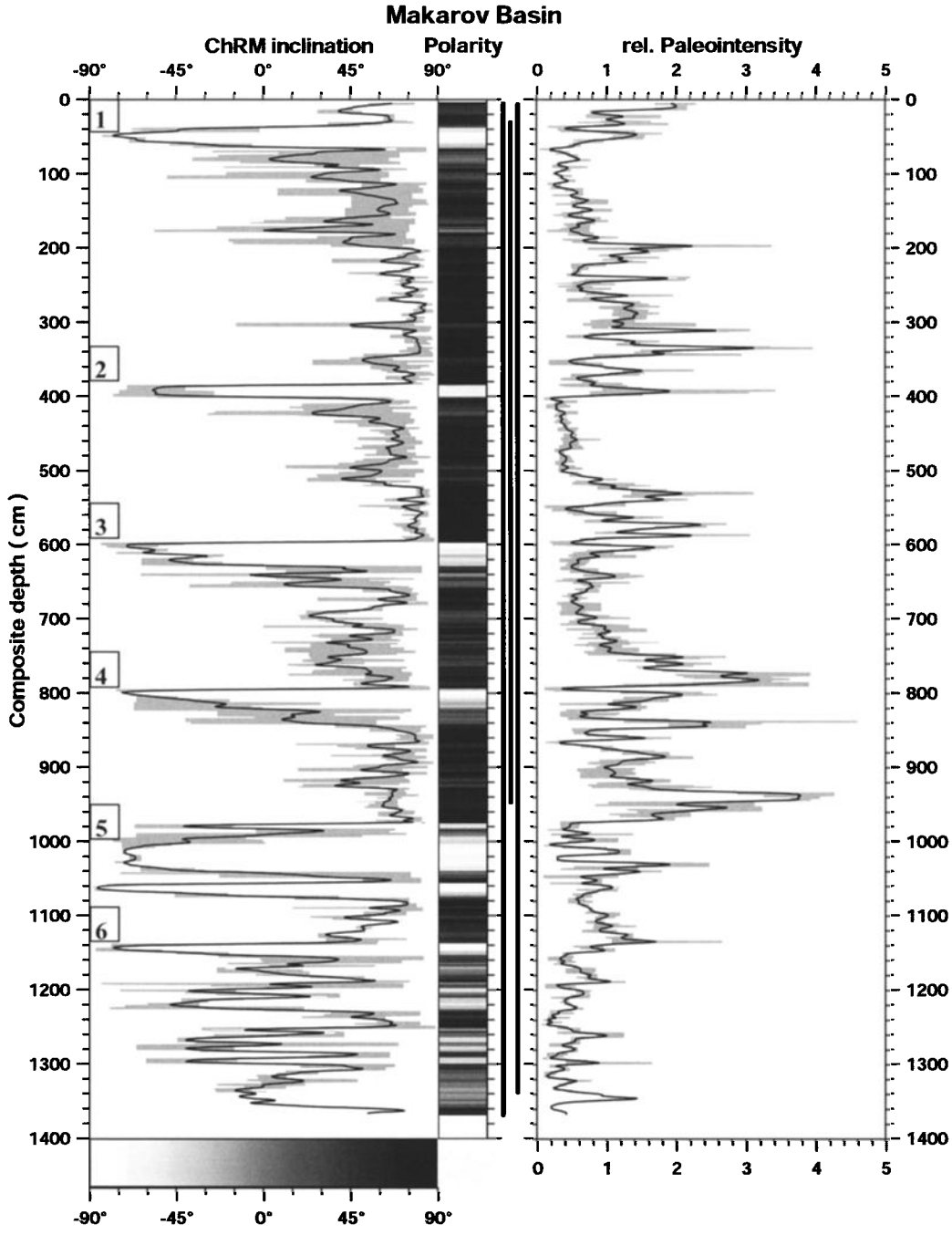

Figure 11. Stacks of the ChRM inclinations (see Figure 2) and relative paleointensity estimates (J_{NRM} (50 mT)/J_{ARM} (50 mT), see Figure 7) as a function of composite depth using the correlation functions shown in Figure 9. The shaded areas underlying both curves indicate the maximum deviations of the individual records from the stacked curves. Vertical lines in the middle indicate the depth intervals covered by cores PS2178-3 (left line), PS2178-5, (middle line), and PS2180-2 (right line). According to the gray scale bar in the bottom left, the inclination pattern was converted into gray values, yielding the "polarity" pattern in the middle. Numbers in boxes mark intervals of reversed magnetizations as discussed in the text.

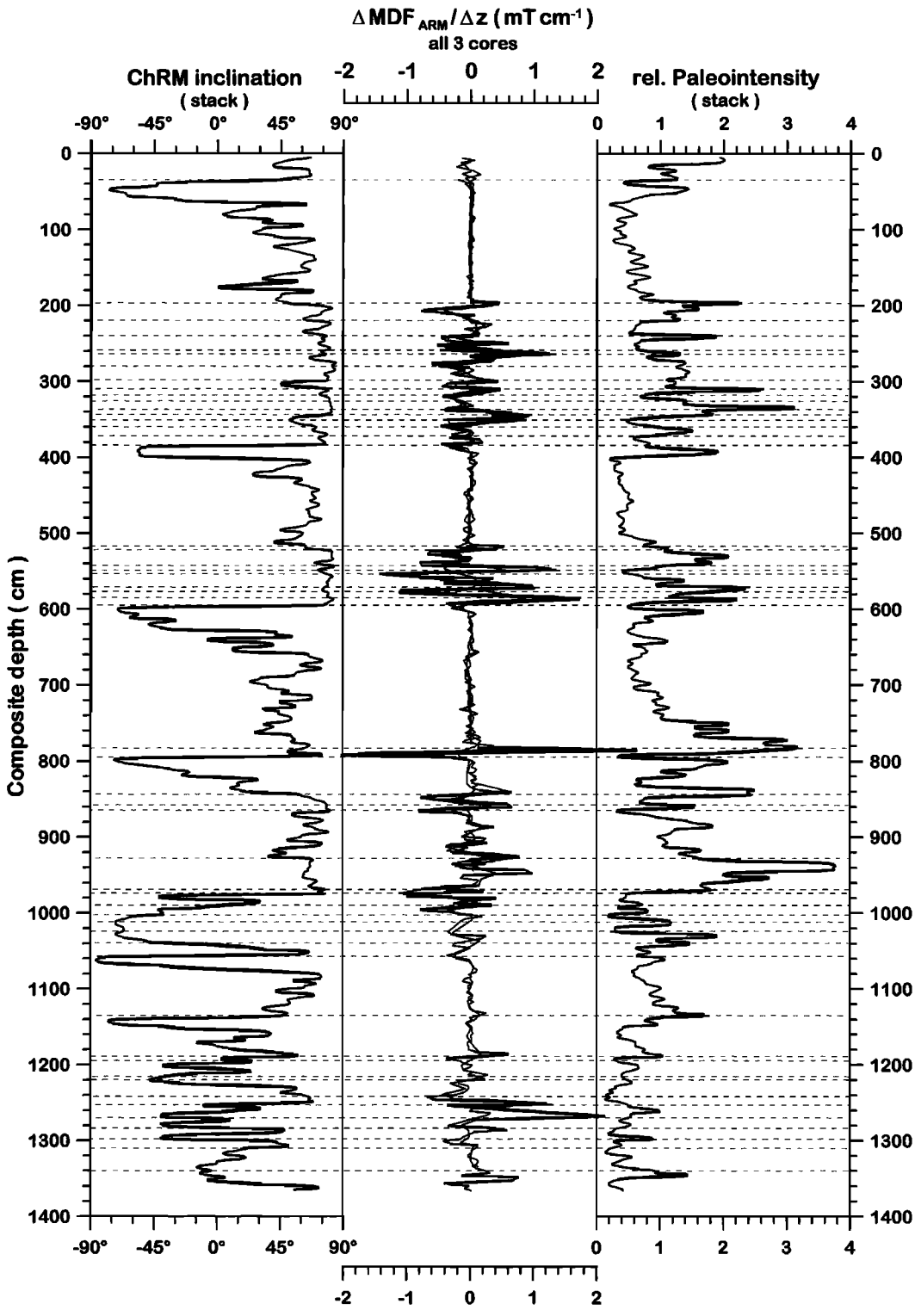

Figure 12. (left) Stack of ChRM inclination, (middle) the ratio $\Delta MDF_{ARM}/\Delta z$, and (right) stack of relative paleointensity. The stacks of ChRM inclination and relative paleointensity are plotted together with the first derivatives of the magnetic grain size indicative median destructive field of the ARM (MDF_{ARM}) of all three cores, approximated by the ratio $\Delta MDF_{ARM}/\Delta z$. The displayed $\Delta MDF_{ARM}/\Delta z$ ratios average over two successive sampling intervals. Ratios that are about equal zero indicate homogeneous sections (compare Figure 10). A single spike within the curves (e.g., at 800 cm) indicates a sudden change in magnetic grain size, possibly a hiatus, whereas successions of spikes (e.g., 190–380 cm) indicate short-scale magnetomineralogic/lithologic variations.

levels the ratios coincide with one another, a basic requirement for a reliable paleointensity estimation [*Tauxe*, 1993]. Dashed lines in Figure 7 indicate the correlation of the three cores based on the paleointensity estimates. In the following discussion the term relative paleointensity refers to the ratio J_{NRM} (50 mT)/J_{ARM} (50 mT). Additional tests of reliability of relative paleointensity are shown in Figure 8. Magnetic susceptibility κ_{LF} exhibits a fairly linear relationship to the ARM intensity J_{ARM} (except for ~7% of the samples), and the SIRM intensity J_{SIRM} is linear with κ_{LF}. There is no visible link between relative paleointensity and magnetic grain size-indicative parameters (Figures 8c and 8d), and also, relative paleointensity variations are related to neither the degree of anisotropy (Figure 8e) nor the shape of the anisotropy ellipsoid (Figure 8f).

4.4. Core Correlation and Creation of Composite Profile

Data of ChRM inclinations (Figure 2), low field magnetic susceptibility κ_{LF}, ARM intensity (Figure 5a), median destructive field of ARM (MDF_{ARM}, Figure 5b), estimates of relative paleointensity (Figure 7), and additional information from sediment color (core photographs) were used to correlate cores PS2178-5 and PS2180-2 to core PS2178-3, yielding the transfer functions shown in Figure 9. Core PS2178-3 is defined as the master core because it covers the longest time interval, and its depth scale is referred to as "composite depth" hereafter.

After transformation to composite depth, the concentration (J_{ARM}) and grain size (MDF_{ARM}) variations of the magnetic minerals match nearly perfectly (Figure 10). Horizontal lines indicate lithology changes derived from inspection of core photographs. The data sets of ChRM inclination and relative paleointensity were also transformed to composite depth (PS2178-3) but were then resampled in intervals of 0.5 cm, stacked, and subsequently smoothed with a weighted (triangular) moving average window of 5.5 cm length (Figure 11). Thick vertical lines in Figure 11 indicate the lengths of the individual cores versus composite depth. Since only three cores were stacked, with 30% of the composite covered by only two cores, we show the minimum and maximum deviation of the individual results from the stack, indicated by shaded areas, instead of giving the standard deviation.

The stacked ChRM inclinations were also transformed to gray values according to the gray scale bar in the lower left of Figure 11. The resulting pseudopolarity pattern shown in the middle of Figure 11 clearly indicates that at least the upper ~10 m are of Brunhes age. The resulting minimum mean sedimentation rate thus calculates to ~1.3 cm kyr^{-1}.

4.5. Quantification of Sediment Variability

The rock magnetic parameters ARM intensity (J_{ARM}), representing the concentration of magnetic particles, and the coercivity parameter median destructive field of ARM (MDF_{ARM}) as a proxy of their relative grain size, show significant patterns. Intervals of constant concentration and constant magnetic grain size alternate with intervals where both parameters show larger fluctuations, e.g., in the top half of the composite profile (Figure 10), or sudden changes from one constant level to a different constant level, e.g., at 1140 and 1305 cm composite depth. All these fluctuations are linked to lithology changes expressed by sediment color and/or texture. In order to quantify the effect of these variations we chose the magnetic grain size-related parameter MDF_{ARM} and calculated the slope of its down core variation with the formula

$$\frac{\Delta MDF_{ARM}}{\Delta z}(n) = \frac{1}{2}\left(\frac{[MDF_{ARM}(n) - MDF_{ARM}(n-1)]}{[z(n) - z(n-1)]} + \frac{[MDF_{ARM}(n+1) - MDF_{ARM}(n)]}{[z(n+1) - z(n)]}\right), \quad (1)$$

where n denotes the sample number. The calculation of the slope in (1) averages over two successive sampling intervals, which was done in order to achieve a slight smoothing effect. The data processing was performed after transformation to the composite depth scale. The results of the individual cores are superimposed in the middle of Figure 12 together with the ChRM inclination and paleointensity stacks. Like in Figure 10, horizontal lines indicate lithology changes derived from inspection of core photographs. Intervals where the slope is about zero (for longer intervals, such as from 40 to 190 cm, 390 to 510 cm, and 590 to 780 cm) represent very homogeneous sections in terms of magnetic concentration and grain size (see Figure 10) with no visible lithology change. A single spike, such as at 800 cm, indicates a sudden change in magnetic grain size, i.e., a change in type and/or rate of sedimentation, possibly even a hiatus. Successions of spikes (e.g., 190–390 cm) indicate short-scale magnetomineralogic (lithologic) variations. Nevertheless, the overall variations are only moderate (see Figures 4 and 5) and still clearly within a range that allows a correct paleointensity reconstruction [e.g., *Tauxe*, 1993]. Therefore the relative paleointensity record from the Makarov Basin can be interpreted also across changes in lithology.

4.6. Radiometric Age Information

Five AMS ^{14}C ages are available from the large box corer taken at Site PS2180 (Table 3 and Figure 13). First, a constant reservoir correction of 440 years was applied to the radiocarbon ages after *Mangerud and Gulliksen* [1975]. However, we expect that the ^{14}C reservoir effect of seawater has been considerably larger and variable during periods of oxygen isotope stages 2 and 3 [*Völker et al.*, 1998]. Radiocarbon ages were converted to calendar ages by the CALIB 4.3 calibration program by using the calibration data sets of *Stuiver et al.* [1998] and *Stuiver and Reimer* [1993] and, beyond 20.3 ^{14}C ka, by applying the age shift determined by *Völker et al.* [1998].

The results indicate low sedimentation rates of ~0.4 cm kyr^{-1} for the last ~40 kyr with slightly higher rates in the Holocene (0.6 cm kyr^{-1}). A linear extrapolation would yield a depth of ~310 cm for the Matuyama Brunhes reversal (780 ka). Obviously, the inclination pattern of the Makarov Basin composite exhibits predominantly normal polarity down to at least 970 cm. According to nannofossil stratigraphy performed on the cores presented in this

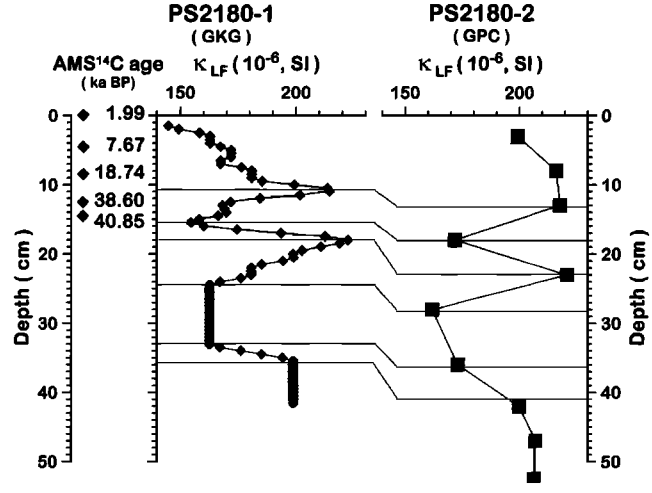

Figure 13. AMS ^{14}C ages of core PS2180-1 (GKG is the box corer) and correlation with core PS2180-2 by means of low field magnetic susceptibility κ_{LF}. The symbol sizes are proportional to the paleomagnetic sample size (PS2180-2) and the interval integrated during spot reading measurement (PS2180-1), respectively.

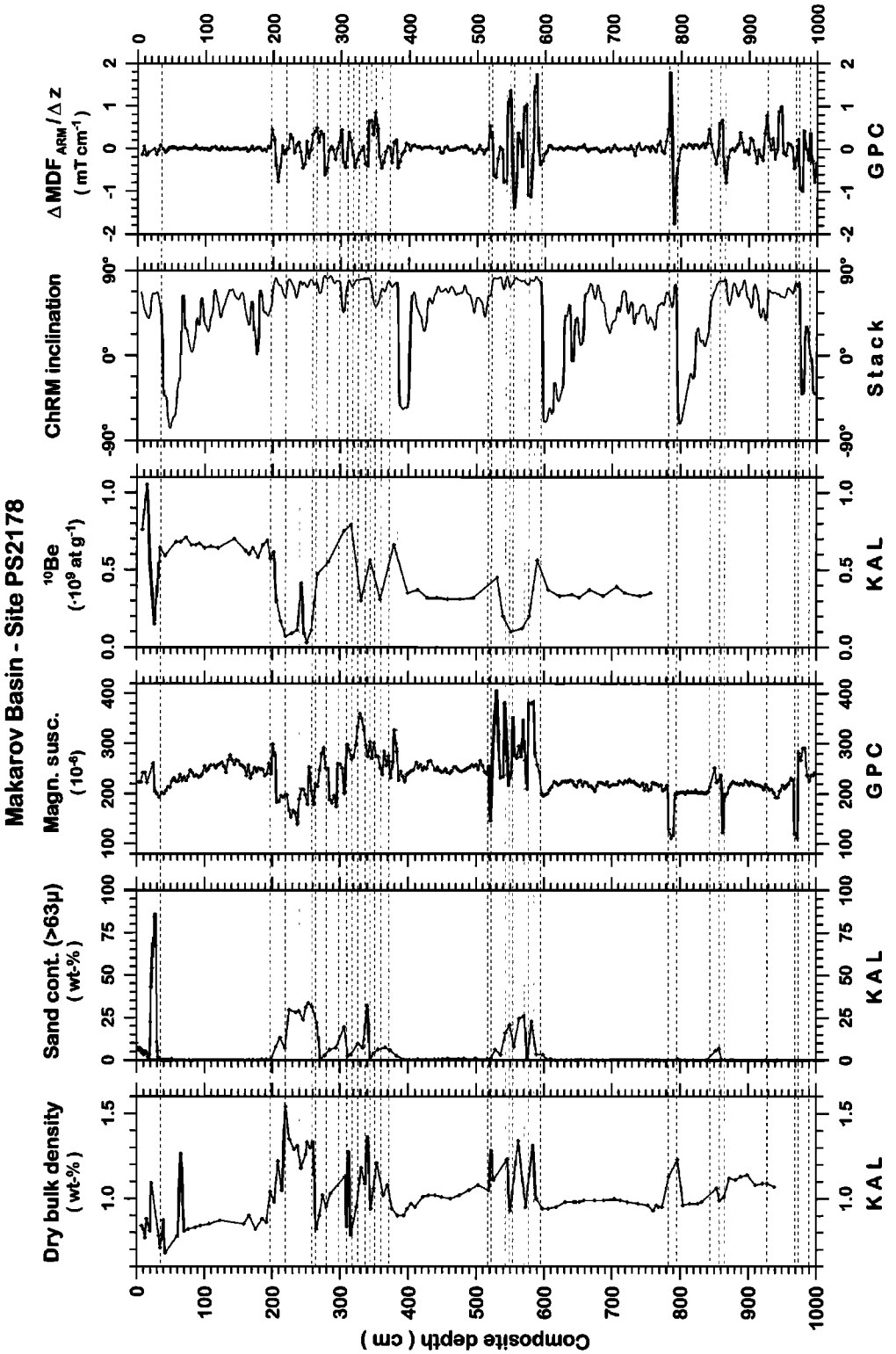

Figure 14. Compilation of available stratigraphic parameters for Site PS2178 versus composite depth: from left to right, dry bulk density (DBD), sand content (>63 µm), magnetic susceptibility, ^{10}Be [*Schäper*, 1994], ChRM inclination, and $\Delta MDF_{ARM}/\Delta z$ ratios. Horizontal lines indicate visible changes in lithology. KAL, data from Kastenlot PS2178-5; GPC, data from giant piston corer PS2178-3.

paper [see *Gard*, 1993, p. 229], "in the Makarov Basin Holocene sediments are about 10 cm deep." Unfortunately, no further precise data, e.g., a plot of the raw data, are given by *Gard* [1993], except a listed sedimentation rate of ~1.4 cm kyr^{-1}. This does not directly contradict the results from AMS ^{14}C dating since coccoliths stratigraphy is a more conceptual dating technique based on several assumptions.

Taking the correlation of the box corer to the piston corer from Site PS2180, the topmost interval of reversed ChRM inclination can be identified as the Laschamp geomagnetic reversal excursion [*Bonhommet and Babkine*, 1967; *Gillot et al.*, 1979]. The Laschamp excursion has been frequently found in Arctic marine sediments as a pronounced paleomagnetic feature, i.e., with thicknesses between 30 and 60 cm, clearly reversed inclinations, extremely low relative paleointensities for transitional directions, and a field strength recovery during its reversed phase [e.g., *Nowaczyk and Baumann*, 1992; *Nowaczyk et al.*, 1994; *Nowaczyk*, 1997; *Nowaczyk and Knies*, 2000]. Another candidate would be the Mono Lake excursion [*Denham and Cox*, 1971; *Liddicoat and Coe*, 1979]. However, detailed studies could not detect a field recovery for this excursion [e.g., *Nowaczyk*, 1997; *Nowaczyk and Knies*, 2000], as was found for the topmost excursion in Makarov Basin sediments (Figure 11). With an age of ~40 ka [*Laj et al.*, 2000] and a maximum duration of ~5–6 kyr, it is spread over 30 cm in core PS2180-2 (Figure 2), yielding sedimentation rates of at least 5 cm kyr^{-1}, 5–10 times higher than for the overlying sediments, when taking the AMS ^{14}C data. Obviously, the depositional conditions at the coring sites in the Makarov Basin were highly variable during the last ~50 kyr.

A ^{10}Be record is established by *Schäper* [1994] for core PS2178-5 (Figure 14) down to 760 cm composite depth (equivalent to 640 cm in core PS2178-5; total length is 831 cm). The ^{10}Be concentration obviously is strongly influenced by lithological changes since its morphology (roughly) parallels the morphologies of the dry bulk density (DBD) and the magnetic susceptibility records, respectively (Figure 14). Intervals that are composed of silty clays, with little changes in lithology, i.e., where DBD, susceptibility, and $\Delta MDF_{ARM}/\Delta z$ are constant, are characterized by only a slight and smooth decay in the ^{10}Be curve, whereas intervals of variable lithology exhibit large distortions in the ^{10}Be curve. Especially within intervals of increased sand content (>63 μm), the ^{10}Be content is strongly reduced. This is normal since ^{10}Be is adsorbed by clay minerals. Fitting an exponential decay curve to the ^{10}Be record of PS2178-5, a maximum mean sedimentation rate of 1.1 cm kyr^{-1} (corrected to composite depth) was estimated by *Schäper* [1994], assuming a constant deposition. However, this can be only a rough estimate since the sedimentation was not constant (see above) both in terms of rate and type of material deposited.

5. Discussion of Age Models

5.1. Age Model 1

On the basis of the identification of excursion 1 as the Laschamp excursion (Figure 11) we correlated the magnetostratigraphic results (relative paleointensity and polarity) from the Makarov Basin to comparable data sets from the Nordic Seas and the North Atlantic (Figure 15). From these reference data sets and the "SINT800" paleointensity stack [*Guyodo and Valet*, 1999] it is known that the intensity minimum in the SINT800 linked to the Laschamp excursion at ~40 ka is preceded by a broad high between 45 and 60 ka, with a maximum at 50 ka. Comparing the morphologies of the paleointensity records, such a maximum is present at ~200–230 cm composite depth in the Makarov Basin record, yielding very high sedimentation rates on the order of 10 cm kyr^{-1}. The interval from 200 to 30 cm (composite depth) of homogeneous sediments reflects a high sedimentation rate event in the Makarov Basin, providing a high-resolution record of the geomagnetic field behavior, i.e., the field intensity decay starting at ~50 ka, followed by the normal-reversed (N-R) transition of the Laschamp reversal excursion. Its abrupt termination (R-N transition) is obviously caused by a drastic decrease in sedimentation rate or, more likely, a hiatus since sediment properties, especially the sand content, change quite drastically above the interval of reversed inclinations (e.g., Figure 14). A similar conclusion can be drawn at least for excursions 2 and 3 at ~400 and 600 cm composite depth, respectively, because they are also situated in the top of homogeneous sediment sequences, overlain by deposits with more heterogeneous properties (Figures 12 and 14). According to the (tentative) correlation shown in Figure 15, excursions 2–4 can be related to the Blake (118 ka), Jamaica (190 ka), and Pringle Falls excursions (220 ka), respectively. As already pointed out by *Nowaczyk and Frederichs* [1999] and *Channell* [1999], the Pringle Falls excursion is not coincident with the "Jamaica excursion" (or Iceland Sea excursion) as concluded by *Langereis et al.* [1997]. Finally, excursion 5 would be related to the Biwa II/Fram Strait excursion (260 ka [*Langereis et al.*, 1997]). From ~1170 cm (composite depth) downward, no clear correlation of the paleointensity record to ODP Site 983 can be achieved. This section is characterized by oscillating flat positive and negative inclinations. According to the correlation shown in Figure 15, an age of ~350–400 ka can be estimated for the bottom of the Makarov Basin composite record, resulting in a mean sedimentation rate in the range of 3–4 cm kyr^{-1}. However, temporal sedimentation rates range from 0.4 to ~5, perhaps even 10, cm kyr^{-1}.

Similar to the results from the Iceland and Greenland Seas, geomagnetic excursions recorded in Makarov Basin sediments are associated with a recovery in relative paleointensity (Figure 15). Brunhes Chron reversal excursions are not present in the majority of other paleointensity records, which are, unfortunately, often based on u channel measurements, which suffer from smoothing owing to the broad sensor characteristics of whole-core magnetometers. In addition, paleointensity estimates are frequently determined on demagnetization levels of 20 or 30 mT, which are, at least in the case of Arctic marine sediments, probably too low to really resolve the primary magnetization, i.e., the real paleointensity variation, in detail. Relative paleointensity curves for sediments from the Greenland Sea would yield a single minimum when based on 20 mT data, which is split into two much lower minima, with a significant maximum in between, when based on 50 mT data [see *Nowaczyk*, 1997].

5.2. Age Model 2

An alternative interpretation of the Makarov Basin magnetostratigraphic record, correlated to ODP Site 1010 in the northeast Pacific [*Hayashida et al.*, 1999], is shown in Figure 16. The polarity transition between 1000 and 970 cm is now related to the Matuyama Brunhes reversal (780 ka). The normal intervals from 1135 to 1070 and 1050 to 1040 cm composite depth can be related to the Jaramillo and Kamikatsura events, respectively. Overall, the Makarov Basin record matches quite well with the ODP Site 1010 record between ~840 and 1150 cm. Especially, the pattern within the 200 cm above the inferred Matuyama Brunhes reversal with its strong increase after the R-N transition appears to be convincing. In light of this alternative interpretation, there should be a clear preference for reversed directions for the lowermost ~2 m of the ChRM inclination stack of the Makarov Basin, as one would expect for pre-Jaramillo (mid-Matuyama) sediments (Figure 16; see also Figure 11). Instead, inclinations are very scattered. So, also in age model 2, no unequivocal correlation to the chosen reference data set is possible for this section of the composite profile.

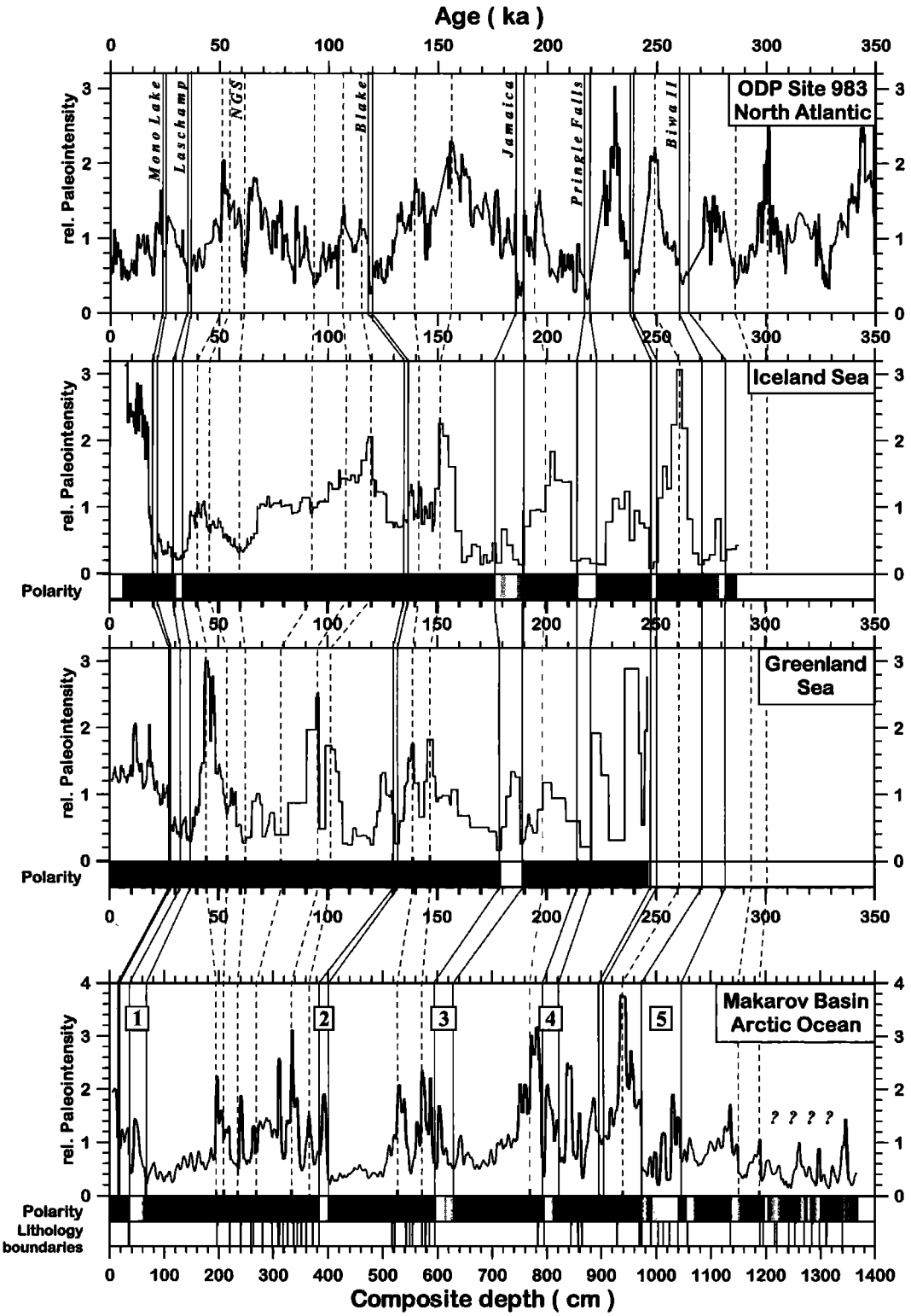

Figure 15. Age model 1: correlation of the magnetostratigraphic results from the Makarov Basin, Arctic Ocean, plotted versus composite depth, to other records from the Greenland Sea [after *Nowaczyk*, 1997], the Iceland Sea [*Nowaczyk and Frederichs*, 1999], and the North Atlantic, Site ODP 983 [*Channell et al.*, 1997], all plotted versus age. Names in the North Atlantic graph indicate geomagnetic excursions; NGS is Norwegian Greenland Sea excursion. Numbers in boxes in the Makarov Basin graph mark intervals of reversed magnetizations as discussed in the text (see also Figure 2).

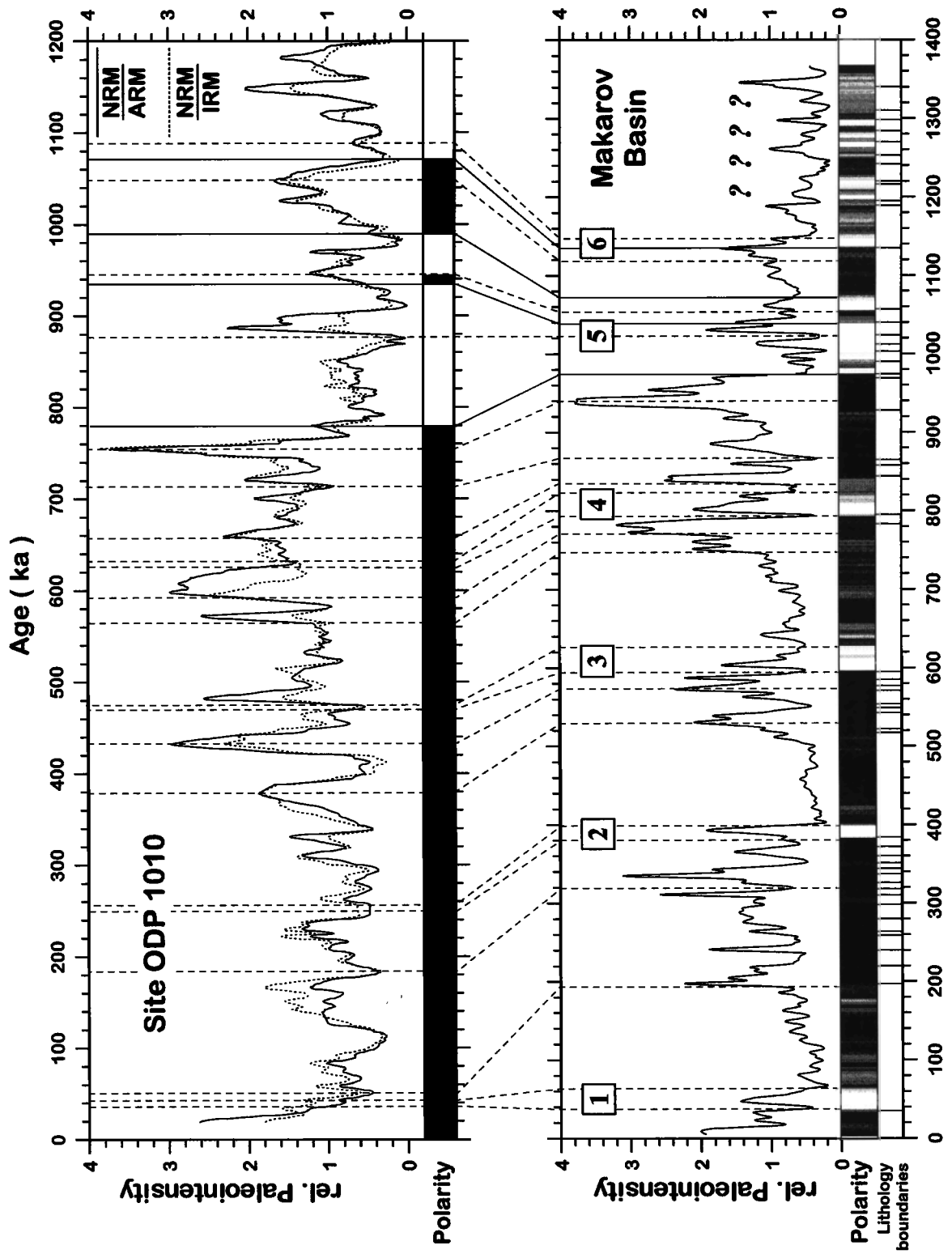

Figure 16. Age model 2: correlation of the relative paleointensity record from the Makarov Basin with the paleointensity record from ODP Site 1010, northeast Pacific [*Hayashida et al.*, 1999]. Numbers in boxes in the Makarov Basin graph mark intervals of reversed magnetizations as shown in Figure 2 and discussed in the text.

According to age model 2, four Brunhes Chron reversal excursions are present in the Makarov Basin record. Their identification is not straightforward since *Langereis et al.* [1997] discuss the presence of 11 and *Lund et al.* [1998] postulate even 14 reversal excursions during the Brunhes Chron. From the available AMS ^{14}C ages it is clear that the reversed section between 35 and 63 cm is a record of the Laschamp reversal excursion at 40 ka. The paleointensity maximum at ~210 cm composite depth should be related to an age of ~50 ka (Figure 13). The identification of the three other reversal excursions (2–4) must be left as tentative since sedimentation rates in the Makarov Basin must be recognized as highly variable, or even noncontinuous, resulting in compression, elongation, or missing of parts of the paleointensity patterns. So, in age model 2, excursion 2 now might relate to the Biwa II/Fram Strait excursion (255–265 ka [*Langereis et al.*, 1997; *Nowaczyk and Frederichs*, 1999]). The identification of excursion 3 (470 ka?) is not clear, whereas excursion 4 with an inferred age of ~615 ka might be related to the La Palma excursion, recently described by *Quidelleur et al.* [1999].

5.3. Comparison of Age Models

The age-depth relationships of the Makarov Basin record for age model 1, based on correlation to ODP Site 983 and other Nordic Seas records (Figure 15), and age model 2, based on correlation to ODP Site 1010 in the northeast Pacific (Figure 16), are shown in Figure 17. Both age models have in common that sedimentation rates are highly variable, and they are nearly identical for about the top 2 m since here AMS ^{14}C ages and the interpretation of the paleomagnetic results are the same. Below ~2 m composite depth both age models result in completely different long-term mean sedimentation rates: ~5 cm kyr^{-1} for age model 1 and only 1 cm kyr^{-1} for age model 2. On one hand, the decay of the ^{10}Be content infers low sedimentation rates on the order of 1 cm kyr^{-1}; that is, this data set favors age model 2. On the other hand, the lowermost 2 m of the composite exhibit too much normal polarity directions. This interval should be characterized by clearly dominating reversed field polarity since it is of middle Matuyama age, according to age model 2. The presence of a high amount of normal polarity data might be an indication that model 1 should be favored, resulting in ages all younger than the Matuyama Brunhes reversal (780 ka). Since the ^{10}Be record is incomplete, no final interpretation can be drawn. Nevertheless, the new results from the Makarov Basin clearly indicate higher long-term mean sedimentation than at the Alpha Ridge (0.1 cm kyr^{-1}) (Table 1) [*Aksu and Mudie*, 1985] and compare more to paleomagnetic results from the eastern Arctic Ocean, e.g., the Nansen Basin (Table 1, minimum of 1 cm kyr^{-1}) [*Nowaczyk and Baumann*, 1992; *Schneider et al.*, 1996], or the Yermak Plateau (3–10 cm kyr^{-1}) [*Nowaczyk et al.*, 1994; *Schneider et al.*, 1996; *Nowaczyk and Knies*, 2000].

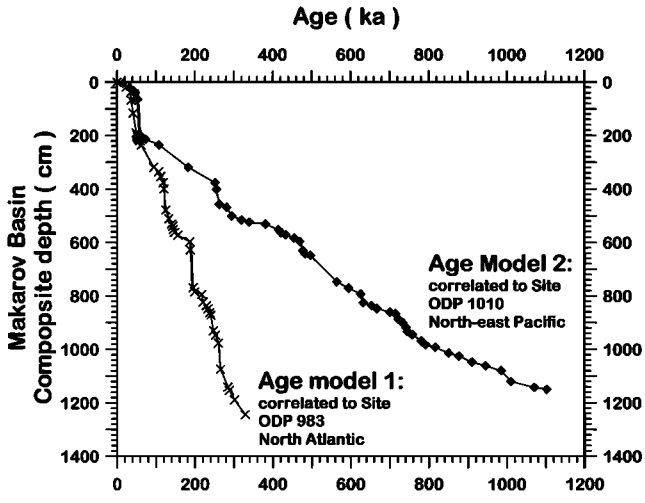

Figure 17. Age-depth curves of the two age models based on the correlations shown in Figures 15 and 16, respectively.

Dating of long sediment cores from the neighboring Lomonosov Ridge is of similar difficulty since here the paleomagnetic results also allow alternative interpretations. Below ~3 m subbottom depth a complex pattern of steep positive and negative inclinations but without a clear preference for reversed or normal polarity was found as well. Depending on where the Matuyama/Brunhes reversal was set, minimum sedimentation rates can be estimated to be either in the range of 0.2 [*Spielhagen et al.*, 1997] or 0.7 cm kyr^{-1} [*Jakobsson et al.*, 2000]. A third age model with interpretation of reversed inclinations as being solely records of short reversal excursion within the Brunhes Chron yields sedimentation rates of the order of 1.4 cm kyr^{-1} [*Frederichs*, 1995]. Sedimentary conditions on top of the Lomonosov Ridge are different from that of the Makarov Basin since winnowing due to water currents passing the crest of this oceanic ridge should lead to reduced sedimentation. Fine-grained material not deposited on top of the ridge should accumulate elsewhere, e.g., in the Makarov Basin, so that comparably high sedimentation rates can be found here. Both age models of this study agree with this.

6. Conclusions

Intervals of steep negative inclinations present in the investigated Makarov Basin sediments are interpreted as records of geomagnetic field behavior, i.e., short reversal excursions [*Gubbins*, 1999] and/or major reversals of the Earth's magnetic field. Reversed inclinations are mainly found in intervals of homogeneous sediments in terms of rock magnetic and sedimentological properties. The overall moderately variable to nearly constant rock magnetic properties provide suitable conditions for reconstruction of relative paleointensity variations and their correlation to dated reference curves. In the recovered Makarov Basin, sediments' relative paleointensities are lowest during polarity transitions, with a recovery in amplitude during the reversed state of the geomagnetic field. Highest values are always linked to clear normal polarity phases. This pattern of high normal polarity field strength, low transitional field strength, and (slight) recovery during clearly reversed polarity of the excursions has been found also in other detailed studies on sediment cores from the Greenland and Iceland Seas [*Nowaczyk*, 1997; *Nowaczyk and Frederichs*, 1999] and the Arctic Ocean [*Nowaczyk and Knies*, 2000]. However, in these records the transitional field intervals with low relative paleointensity amplitudes were much shorter with a more or less instantaneous change from normal to reversed inclinations and back. Compared to this, the onsets of the excursions are spread over quite a long interval characterized by a broad low in relative paleointensity with ChRM inclinations oscillating rather than switching instantaneously from normal to reversed. The terminations of the excursions are often quite sharp. They coincide in general with changes in lithology, i.e., changes in type of sediment and rate of deposition, or even hiatuses. Obviously, the asymmetrical pattern of the directional as well as amplitudinal behavior of the paleomagnetic signal is rather caused by a highly variable sedimentation than by geomagnetic field behavior. This has to be taken into account when correlating the paleomagnetic results from Makarov Basin to reference data sets since the fairly well established patterns of relative paleointensity record, such as the SINT800 stack, should be largely elongated or compressed depending on the current sedimentation rate. Correlations to available reference curves allow two different interpretations of

the Makarov Basin paleomagnetism, i.e., inclination and relative paleointensity record. Both models result in highly variable sedimentation rates but with different maximum values. Interpreting all documented reversed directions as excursional features yields a mean sedimentation rate in the range of 4 cm kyr^{-1} and an age of ~400 ka for the bottom of the composite section (age model 1). An alternative interpretation yields a mean sedimentation rate in the range of 1.3 cm kyr^{-1}, an age of at least ~1.2 Ma, for the bottom of the Makarov Basin record. The available, unfortunately incomplete, ^{10}Be record favors the low sedimentation interpretation, but the low amount of clearly reversed direction in the bottom of the section does the opposite. Thus unless no further high-quality long cores exceeding the present Makarov Basin record are available, this question must be left open.

7. Data Availability

Paleomagnetic and rock magnetic data are accessible at http://www.pangaea.de/PangaVista. Enter search option Nowaczyk +2001 +Makarov (with a space before each plus). The data from cores PS2178-3, PS2178-5, and PS2180-2 comprise depth; composite depth (PS2178-3); ages according to age models 1 and 2; NRM intensity J_{NRM}; ChRM inclination and declination; low field susceptibility κ_{LF}; ARM intensity J_{ARM}; MDF_{ARM}; κ_{ARM}/κ_{LF}; J_{NRM} (50 mT)/κ_{LF}, same with 3 point weighted running average; and J_{NRM} (50 mT)/J_{ARM} (50 mT), same with 3 point weighted running average. Additional data are available for core PS2180-2 only: SIRM intensity (J_{SIRM}); J_{NRM} (50 mT)/J_{SIRM}, same with 3 point weighted running average; mean susceptibility determined from anisotropy ellipsoid plus standard error; principle anisotropy axes K_{max}, K_{int}, and K_{min}; inclination and declination of K_{max}, K_{int}, K_{min}; and degree ($100(K_{max} - K_{min})/K_{max}$) and shape ($K_{max}K_{min}/K_{int}^2$) of anisotropy ellipsoid. Color photographs of core PS2178-3 are available as a pdf file. Data for Makarov Basin stack comprise ChRM inclination and paleointensity based on J_{NRM} (50 mT)/J_{ARM} (50 mT).

Acknowledgments. We thank the captain and the crew of R/V *Polarstern* for cooperation during expedition ARK VIII/3. L. Brück and C. Müller helped during laboratory work in Bremen and Potsdam. We also would like to thank Y. Guyodo, J. E. T. Channell, and A. Hayashida for providing their paleointensity data sets. John King and two other ambitious reviewers are acknowledged for their constructive comments on the manuscript. This study was partly financed by the Bundesministerium für Forschung und Technologie, Germany.

References

Aksu, A. E., and P. J. Mudie, Magnetostratigraphy and palynology demonstrates at least 4 million years of Arctic Ocean sedimentation, *Nature, 318*, 280–283, 1985.

Bleil, U., Magnetostratigraphy of Neogene and Quaternary sediment series from the Norwegian Sea: Ocean Drilling Program, Leg 104, *Proc. Ocean Drill. Program Sci. Results, 104*, 829–850, 1989.

Bleil, U., and G. Gard, Chronology and correlation of Quaternary magnetostratigraphy and nannofossil biostratigraphy in Norwegian-Greenland Sea sediments, *Geol. Rundsch., 78*, 1173–1187, 1989.

Bonhommet, N., and J. Babkine, Sur la présence d'aimantations inversées dans la Chaîne des Puys, *C. R. Acad. Sci., 264*, 92–94, 1967.

Channell, J. E. T., Geomagnetic paleointensity and directional secular variation at Ocean Drilling Program (ODP) Site 984 (Bjorn Drift) since 500 ka: Comparison with ODP Site 983 (Gardar Drift), *J. Geophys. Res., 104*, 22,923–22,951, 1999.

Channell, J. E. T., D. A. Hodell, and B. Lehman, Relative geomagnetic paleointensity and $\delta^{18}O$ at ODP Site 983 (Gardar Rift, North Atlantic) since 350 ka, *Earth Planet. Sci. Lett., 153*, 103–118, 1997.

Channell, J. E. T., J. S. Stoner, D. A. Hodell, and C. D. Charles, Geomagnetic paleointensity for the last 100 kyr from the sub-antarctic South Atlantic: A tool for inter-hemispheric correlation, *Earth Planet. Sci. Lett., 175*, 145–160, 2000.

Clark, D. L., R. R. Whitman, K. A. Morgan, and S. D. Mackey, Stratigraphy and glacial-marine sediments of the Amerasian Basin, central Arctic Ocean, *Spec. Pap. Geol. Soc. Am., 181*, 57 pp., 1980.

Coles, R. L., and P. T. Taylor, Magnetic anomalies, in *The Arctic Ocean Region, The Geology of North America, vol. L*, edited by A. Grantz, L. Johnson, and J. F. Sweeney, pp. 119–132, Geol. Soc. of Am., Boulder, Colo., 1990.

Darby, D. A., A. S. Naidu, T. C. Mowatt, and G. Jones, Sediment composition and sedimentary processes in the Arctic Ocean, in *The Arctic Seas: Climatology, Oceanography, Geology, and Biology*, edited by Y. Hermann, pp. 657–720, Van Nostrand Reinhold, New York, 1989.

Denham, C. R., and A. Cox, Evidence that the Laschamp polarity event did not occur 13300-30400 years ago, *Earth Planet. Sci. Lett., 13*, 181–190, 1971.

Frederichs, T., Regional and temporal variations of rock magnetic parameters in Arctic marine sediments (in German with English abstract), *Rep. Polar Res., 164*, 212 pp., 1995.

Gard, G., Late Quaternary coccoliths at the North Pole: Evidence of ice-free conditions and rapid sedimentation in the central Arctic Ocean, *Geology, 21*, 227–230, 1993.

Gillot, P. Y., J. Labeyrie, C. Laj, G. Valladas, G. Guérin, G. Poupeau, and G. Delibrias, Age of the Laschamp paleomagnetic excursion revisited, *Earth Planet. Sci. Lett., 42*, 444–450, 1979.

Grantz, A., S. D. May, P. T. Taylor, and L. A. Lawver, Canada Basin, in *The Arctic Ocean Region, The Geology of North America, vol. L*, edited by A. Grantz, L. Johnson, and J. F. Sweeney, pp. 379–402, Geol. Soc. of Am., Boulder, Colo., 1990.

Gubbins, D., The distinction between geomagnetic excursions and reversals, *Geophys. J. Int., 137*, F1–F3, 1999.

Guyodo, Y., and J.-P. Valet, Global changes in intensity of the Earth's magnetic field during the past 800 kyr, *Nature, 399*, 249–252, 1999.

Hayashida, A., K. L. Verosub, F. Heider, and R. Leonhardt, Magnetostratigraphy and relative palaeointensity of late Neogene sediments at ODP Leg 167 Site 1010 off Baja California, *Geophys. J. Int., 139*, 829–840, 1999.

Jackson, H. R., D. A. Forsyth, J. K. Hall, and A. Overton, Seismic reflection and refraction, in *The Arctic Ocean Region, The Geology of North America, vol. L*, edited by A. Grantz, L. Johnson, and J. F. Sweeney, pp. 153–170, Geol. Soc. of Am., Boulder, Colo., 1990.

Jokat, W., et al., ARCTIC '98: The Expedition ARK-XIV/1a of RV "*Polarstern*" in 1998, *Rep. Polar Res., 308*, 100– 104, 1999.

Jakobsson, M., R. Løvlie, H. Al-Hanbali, E. Arnold, J. Backman, and M. Mörth, Manganese and color cycles in Arctic Ocean sediments constrain Pleistocene chronology, *Geology, 28*(1), 23–26, 2000.

Kirschvink, J. L., The least-squares line and plane and the analysis of palaeomagnetic data, *Geophys. J. R. Astron. Soc., 62*, 699–718, 1980.

Knies, J., N. Nowaczyk, C. Müller, R. Stein, and C. Vogt, A multiproxy approach to reconstruct the environmental changes along the Eurasian continental margin over the last 150,000 years, *Mar. Geol., 163*, 317–344, 2000.

Köhler, S. E. I., Spätquartäre paläo-ozeanographische Entwicklung des Nordpolarmeeres und Europäischen Nordmeeres anhand von Sauerstoff- und Kohlenstoffisotopenverhältnissen der planktischen Foraminifere Neogloboquadrina pachiderma (sin.). *Rep. 13*, 102 pp., GEOMAR, Kiel, Germany, 1992.

Laj, C., C. Kissel, A. Mazaud, J. E. T. Channell, and J. Beer, North Atlantic palaeointensity stack since 75 ka (NAPIS75) and the duration of the Laschamp event, *Philos. Trans. R. Soc. London, Ser. A, 358*, 1009–1025, 2000.

Langereis, C. G., M. J. Dekkers, G. J. de Lange, M. Paterne, and P. J M. Santvoort, Magnetostratigraphy and astronomical calibration of the last 1.1 Myr from eastern Mediterranean piston core and dating of short events in the Brunhes, *Geophys. J. Int., 129*, 75–94, 1997.

Liddicoat, J. C., and R. S. Coe, Mono Lake geomagnetic excursion, *J. Geophys. Res., 84*, 261–271, 1979.

Løvlie, R., B. Markussen, H. P. Sejrup, and J. Thiede, Magnetostratigraphy in three Arctic Ocean sediment cores: Arguments for geomagnetic excursions within oxygen-isotope stage 2-3, *Phys. Earth Planet Inter., 43*, 173–184, 1986.

Lund, S. P., G. Acton, M. Hastedt, and T. Williams, Geomagnetic field excursions occurred often during the last million years, *Eos Trans. AGU, 79*(14), 178–179, 1998.

Mangerud, J., and S. Gulliksen, Apparent radiocarbon ages of recent marine shell from Norway, Spitsbergen, and Arctic Canada, *Quat. Res., 5*, 273–296, 1975.

Merril, R. T., and M. W. McElhinny, The Earth's

magnetic field, its history, origin and planetary perspective, Academic, San Diego, Calif., 1983.

Mienert, J., L. A. Mayer, G. A. Jones, and J. W. King, Physical and acoustic properties of Arctic Ocean deep-sea sediments: Paleoclimatic implications, in *Geological History of the Polar Oceans: Arctic Versus Antarctic, NATO ASI Ser., Ser. C, vol 308*, edited by U. Bleil and J. Thiede, pp. 455–473, Kluwer Acad., Norwell, Mass., 1990.

Morris, T. H., L. D. Clark, and S. M. Blasco, Sediments of the Lomonosov Ridge and Makarov Basin: A Pleistocene stratigraphy for the North Pole, *Geology, 96*, 901–910, 1985.

Nowaczyk, N. R., High-resolution magnetostratigraphy of four sediment cores from the Greenland Sea, II, Rock magnetic and paleointensity data, *Geophys. J. Int., 131*, 325–334, 1997.

Nowaczyk, N. R., and M. Antonow, High-resolution magnetostratigraphy of four sediment cores from the Greenland Sea, I, Identification of the Mono Lake excursion, Laschamp and Biwa I/Jamaica geomagnetic polarity events, *Geophys. J. Int., 131*, 310–324, 1997.

Nowaczyk, N. R., and M. Baumann, Combined high-resolution magnetostratigraphy and nannofossil biostratigraphy for late Quaternary Arctic Ocean sediments, *Deep Sea Res., 39*, 567–601, 1992.

Nowaczyk, N. R., and T. W. Frederichs, Geomagnetic events and relative paleointensity variations during the last 300 ka as recorded in Kolbeinsey Ridge sediments, Iceland Sea—Indication for a strongly variable geomagnetic field, *Int. J. Earth Sci., 88*, 116–131, 1999.

Nowaczyk, N. R., and J. Knies, Magnetostratigraphic results from eastern Arctic Ocean—AMS ^{14}C ages and relative palaeointensity data of the Mono Lake and Laschamp geomagnetic reversal excursions, *Geophys. J. Int., 140*, 185–197, 2000.

Nowaczyk, N. R., T. W. Frederichs, A. Eisenhauer, and G. Gard, Magnetostratigraphic data from late Quaternary sediments from the Yermak Plateau, Arctic Ocean: Evidence for four geomagnetic polarity events within the last 170 Ka of the Brunhes Chron, *Geophys. J. Int., 117*, 453–471, 1994.

Quidelleur, X., P.-Y. Gillot, J. Carlut, and V. Courtillot, Link between excursions and palaointensity inferred from abnormal field directions recorded at La Palma around 600 ka, *Earth. Planet. Sci. Lett, 168*, 233–242, 1999.

Reimnitz, E., L. J. Marincovich, M. McCormick, and W. M. Briggs, Suspension freezing of bottom sediment and biota in the Northwest Passage and implications for Arctic Ocean sedimentation, *Can J. Earth Sci., 29*, 693–703, 1992.

Rothrock, D., et al., Arctic Ocean science from submarines—A report based on the SCICEX 2000 Workshop, pp. 7–9, Appl. Phys. Lab., Univ. of Wash., Seattle, 1999.

Schäper, S., Quartäre Sedimentation im polnahen Arktischen Ozean, diploma thesis, 113 pp., Univ. of Heidelberg, Heidelberg, Germany, 1994.

Schneider, D. A., J. M. F. Backman, W. B Curry, and G. Possnert, Paleomagnetic constraints on sedimentation rates in the eastern Arctic Ocean, *Quat. Res., 46*, 62–71, 1996.

Schubert, C., and R. Stein, Deposition of organic carbon in Arctic Ocean sediments: Terrigenous supply vs marine productivity, *Org. Geochem., 4*, 421–436, 1996.

Scott, D. B., P. J. Mudie, V. Baki, K. D. MacKinnon, and F. E. Cole, Biostratigraphy and late Cenozoic paleoceanography of the Arctic Ocean: Foraminiferal, lithostratigraphic, and isotopic evidence, *Geol. Soc. Am. Bull., 101*, 260–277, 1989.

Smith, J. D., and J. H. Foster, Geomagnetic reversal in Brunhes normal polarity epoch, *Science, 163*, 565–567, 1969.

Spielhagen, R., et al., Arctic Ocean evidence for late Quaternary initiation of northern Eurasian ice sheets, *Geology, 25*(9), 783–786, 1997.

Stein, R., S.-I. Nam, C. Schubert, C. Vogt, D. Fütterer, and J. Heinemeier, The last deglaciation event in the eastern central Arctic Ocean, *Science, 264*, 692–696, 1994a.

Stein, R., C. Schubert, C. Vogt, and D. Fütterer, Stable isotope stratigraphy, sedimentation rates, and salinity changes in the latest Pleistocene to Holocene eastern central Arctic Ocean, *Mar. Geol., 119*, 333–355, 1994b.

Stoner, J. S., J. E. T. Channell, C. Hillaire-Marcel, and C. Kissel, Geomagnetic paleointensity and environmental record from Labrador Sea core MD95-2024: Global marine sediment and ice core chronostratigraphy for the last 100 kyr, *Earth. Planet. Sci. Lett., 183*, 161–173, 2000.

Stuiver, M., and P. J. Reimer, Extended ^{14}C database and revised CALIB radiocarbon calibration program, *Radiocarbon, 35*, 215–230, 1993.

Stuiver, M., P. J. Reimer, E. Bard, J. W. Beck, G. S. Burr, K. A. Hughen, B. Kromer, F. G. McCormac, J. van der Plicht, and M. Spurk, INTCAL98 radiocarbon age calibration, 24,000-0 cal BP, *Radiocarbon, 40*, 1041–1083, 1998.

Sweeney, J. F., G. L. Johnson, and A. Grantz, Summary, in *The Arctic Ocean Region, The Geology of North America, vol. L*, edited by A. Grantz, L. Johnson, and J. F. Sweeney, pp. 619–626, Geol. Soc. of Am., Boulder, Colo., 1990.

Tauxe, L., Sedimentary records of relative paleointensity of the geomagnetic field: Theory and practice, *Rev Geophys., 31*, 319–354, 1993.

Tauxe, L., and J.-P. Valet, Relative paleointensity of the Earth's magnetic field from marine sedimentary records: A global perspective, *Phys. Earth Planet. Inter., 56*, 59–68, 1989.

Völker, A. H. L., M. Sarnthein, P. M. Grootes, H. Erlenkeuser, C. Laj, A. Mazaud, M.-J. Nadeau, and M. Schleicher, Correlation of marine ^{14}C ages from the Nordic Seas with the GISP2 isotope record: Implications for ^{14}C calibration beyond 25 ka, *Radiocarbon, 40*, 517–534, 1998.

Weber, J. R., and J. F. Sweeney, Ridges and basins in the central Arctic Ocean, in *The Arctic Ocean Region, The Geology of North America, vol. L*, edited by A. Grantz, L. Johnson, and J. F. Sweeney, pp. 305–336, Geol. Soc. of Am., Boulder, Colo., 1990.

T. W. Frederichs, Fachbereich Geowissenschaften, Universität Bremen, Postfach 330440, Bremen, D-28443 Germany.

H. Kassens, N. Nørgaard-Pedersen, and R. F. Spielhagen, GEOMAR, Wischhofstrasse 1-3, Kiel, D-24148 Germany.

N. R. Nowaczyk, GeoForschungsZentrum Potsdam, Projektbereich 3.3, Laboratory for Paleo- and Rock Magnetism, Telegrafenberg, Potsdam, D-14473 Germany. (nowa@gfz-potsdam.de)

R. Stein and D. Weiel, Alfred-Wegener-Institute for Polar and Marine Research, Columbusstrasse, Bremerhaven, D-27568 Germany.

(Received March 3, 2000;
revised February 20, 2001;
accepted March 26, 2001.)